DEFECTS IN AMORPHOUS SiO_2:
REACTIONS, DYNAMICS AND OPTICAL PROPERTIES

By

Tamás Bakos

Dissertation
Submitted to the Faculty of the
Graduate School of Vanderbilt University
in partial fulfillment of the requirements
for the degree of

DOCTOR OF PHILOSOPHY

in

Physics

December, 2003

Nashville, Tennessee

Approved:
Prof. Sokrates T. Pantelides
Prof. David J. Ernst
Prof. Leonard C. Feldman
Prof. Daniel M. Fleetwood
Prof. Ronald D. Schrimpf

ACKNOWLEDGMENTS

I am indebted to my thesis advisor, Prof. Sokrates T. Pantelides for guidance, support and training I have received during my dissertation research. Also, I would sincerely like to thank my friend and colleague, Dr. Sergey N. Rashkeev, for his encouragement and help in completing my research.

I would further like to acknowledge valuable discussions and insights I have received from members of our Solid-State Theory Group, Dr. Zhonggy Lu, Dr. Leonidas Tsetseris, Dr. Sanwu Wang and from the Radiation Effects and Reliability Group, especially Profs. Ronald D. Schrimpf and Daniel M. Fleetwood.

I am grateful to the members of my PhD Committee, David J. Ernst, Leonard C. Feldman, Daniel M. Fleetwood and Ronald D. Schrimpf for careful reading and correcting the thesis.

The research described in this dissertation has been sponsored in part through the AFOSR Grant No. F-49620-99-1-0289 with Vanderbilt University.

TABLE OF CONTENTS

Page

Chapter

LIST OF TABLES

LIST OF FIGURES

CHAPTER I

OVERVIEW

Amorphous silicon dioxide is a key component of metal-oxide semiconductor field-effect transistors (MOSFETs), solar cells and optical fibers, all of which are basic elements of modern technology. Practical applications are often limited by various defects that can change the mechanical, electrical and optical properties of the oxide.

This thesis focuses on the behavior of various defects in amorphous SiO_2 with an emphasis on defects that are related to water and oxygen molecules. The results are centered around two main topics: the reactions and dynamics of water and oxygen interstitials in amorphous SiO_2 and the optical properties of two selected defects of technological importance that may form primarily in irradiated SiO_2 that has been exposed to water.

The theoretical approach is based on state-of-the-art first-principles density-functional theory combined with pseudopotentials to describe the interaction between the electrons and the ionic cores, the generalized gradient approximation for exchange and correlation and supercells to characterize the amorphous solid. This calculational method has been tested on a wide variety of Si-O-H systems and has a long track record of successful applications.

a) First, we analyze the properties of water and oxygen molecules brought into contact with bulk silicon-dioxide. Water and oxygen molecules are known to play important roles in determining the properties of amorphous SiO_2, like the growth rate of films on silicon, mechanical strength of silica glass, the rate of structural relaxation, static fatigue and also certain aspects of radiation hardness. Despite the tremendous experimental and theoretical efforts intended to explain how water and oxygen molecules incorporate into, diffuse, and react with amorphous SiO_2, the relevant atomic-scale configurations and processes remain uncertain. For example, there exists no detailed account of whether these molecules remain intact in the interstitial regions, if they diffuse as molecules without breaking up, and if they attach whole to the network or break up in one or more ways.

We show that the behavior of H_2O and O_2 molecules is much more versatile in an amorphous environment than one normally encounters in crystals. For example, diffusion of H_2O is possible through six-member and larger rings with small energy barrier ($\sim$0.8 eV), but it is very unlikely in smaller rings, where the barrier is much higher. On the other hand, when in a diffusion dead-end, an H_2O molecule is more likely to break up at an O atom site, resulting in two silanol groups. In turn, an H_2O molecule can reform on the other side of the ring, allowing diffusion by a novel and unusual "reactive cut" through the network.

In addition, we show that interstitial H_2O and O_2 molecules are viable entities in the voids of the amorphous SiO_2 structure and describe their equilibrium configurations in such voids. We find that an interstitial water molecule may participate in several reactions with the amorphous network, but only the formation of adjacent silanol (Si-OH) groups has a sufficiently low formation energy and activation barrier. Two water molecules may also exist in the bigger voids of the oxide, and, after overcoming a barrier of similar height, they may form H_3O^+ and OH^- defect complexes that may contribute to the fixed charge of bulk SiO_2.

We also study the reactions of water and oxygen molecules with neutral and charged oxygen vacancies (E' centers). E' centers and their precursor defects –neutral oxygen vacancies– are important defects especially in gate oxides because they may act as charge traps and thereby introduce changes in relevant MOSFET characteristics. In optical fibers these centers degrade transmittance by introducing undesirable absorption bands. Experimental observations find that the concentration of E' centers that form under strong irradiation of bulk SiO_2 is dependent on the type of the oxide, especially on the presence or absence of hydroxyl groups ("wet" vs. "dry" oxides). We show that this concentration dependence is related to the different nature and energy barrier of processes by which the E' center is annihilated in wet and dry oxides. In particular, we find that in wet oxides the E' center annihilation is reaction limited (by a 1.3 eV energy barrier) and charged vacancies are annihilated easier than neutral ones, whereas in dry oxides the annihilation of E' centers is diffusion limited with a lower activation barrier of $\sim$ 1 eV that corresponds to the diffusion barrier of O_2 molecules. As a result, heavily irradiated dry oxides will have a smaller concentration of E' centers than wet oxides when irradiated with the same total dose.

As opposed to water, oxygen molecules are more inert in bulk and do not react with the network. We show that they diffuse as interstitial molecules with an energy barrier that is very sensitive to the local ring topology. At the interfaces, however, the energy barrier for the formation of ozonyl (Si-O-O-O-Si) linkages becomes comparable to the diffusion barrier, thus enabling reactions between interstitial O_2 molecules and the SiO_2 network. The reverse reaction is also possible: two oxygen atoms from the ozonyl linkage may form an oxygen molecule that may continue to migrate, similarly to the "reactive cut" diffusion mechanism of water molecules. We suggest that the opening of this reaction channel at the interfaces explains the observed isotope exchange between O_2 and SiO_2.

b) The second part of the results is centered around the optical properties of two particular defects. One of them, an oxygen-excess center, known as non-bridging oxygen, can form only in amorphous SiO_2 (it is essentially a "dangling oxygen"), and has long been associated with a luminescence line at 1.9 eV. The other is an interstitial hydroxyl group (OH_i) in different bonding arrangements that can, in principle, exist in both crystalline and amorphous SiO_2.

Based on the properties of these two defects, we demonstrate a novel phenomenon that occurs only in the solid state: Stokes shifts caused by slow electronic relaxations. Stokes shifts have long been known and attributed to slow atomic relaxations in molecules and solids on the grounds that electronic transitions are fast (Franck-Condon principle). The slow electronic relaxation process, a form of "electronic" Franck-Condon shift, basically comprises the non-radiative "bubbling up" of a deep hole in the valence band to the valence-band edge via a cascade of electron-phonon transitions and is unique to the solid state since it requires a continuum of higher-lying valence states to be present. This electronic relaxation process is associated with a charge reconstruction within the defect and the surrounding solid that takes place between the optical absorption and luminescence processes. This process is of particular importance in determining Stokes shifts between optical excitation and photoluminescence and complements the Stokes-shift caused by atomic relaxations of the defects or of the surrounding solid. The described electronic relaxation process is not only restricted to the above two defects, but quite possibly has a wide applicability for various defects in different media.

In particular, we show that both defects have a partially occupied shallow acceptor level in the SiO_2 band gap, giving rise to a similar optical excitation spectrum. Calculating the optical matrix elements, we find that excitations originate with highest probability from deep valence levels. Thus, a deep hole is created in the valence band in the excitation process. The most likely scenario for the fate of this deep hole is a slow, non-radiative bubbling up to the SiO_2 valence band edge. We analyze this process in detail, showing the participating electronic states and the accompanying charge reconstruction inside the SiO_2 valence band. Once this hole is at the top of the valence band, we show that the ensuing photoluminescence energies are similar, although the luminescence energy is site-dependent in the case of the OH_i defect. We investigate the atomic relaxation of the excited OH_i defect that is responsible for the broadening of the luminescence spectrum.

The optical properties of the hydroxyl group and the non-bridging oxygen are overlapping in amorphous SiO_2, thus raising questions about the proper identification of the latter as the defect responsible for the well-known red photoluminescence line in irradiated, high OH-containing oxides. Since interstitial OH groups may be created in such oxides by irradiation, there is a clear possibility that the OH_i is responsible for at least some of the observations. We suggest new experimental investigations to clarify the properties and roles of these defects.

The thesis is structured as follows. In Chapter II we give a brief outline to the structure of amorphous SiO_2 and describe general some concepts about its defects. We give a short introduction to some of the most relevant defects that have been studied in the literature. In Chapter III an outline of the theoretical background that serves as a foundation of our calculations is given. This chapter also describes the specifications of the VASP software package that we have used in our calculations. We give a short introduction to density functional and pseudopotential theory and describe how the Kohn-Sham equations that give a quantum mechanical treatment of the electronic structure lead to a set of classical equations of motion for the ions in a solid. In a separate section we outline how amorphous systems can be modelled using the supercell approach.

After the preliminaries in Chapters II and III, the original contributions of this work follow. We describe the behavior of water and oxygen molecules in amorphous SiO_2 in

Chapter IV. Chapter V is devoted to the description of the optical properties of the NBO and OH_i defect and of the electronic Franck-Condon shift.

CHAPTER II

INTRODUCTION

Amorphous silicon-dioxide has been one of the most intensively studied materials in materials science and condensed matter physics. The main driver for this intense effort is its critical role in the metal-oxide-semiconductor field effect transistor (MOSFET), which dominates contemporary integrated circuit (IC) technology. Amorphous SiO_2 is also a material of choice for, e.g., optical fibers and solar cells, making its role in modern technology even more important.

This chapter gives a brief introduction to the structure of high-purity crystalline and amorphous SiO_2 and also discusses the nature and properties of defects that have been encountered in these materials.

Review of SiO_2 structures

Crystalline SiO_2

X-ray diffraction experiments[1, 2] reveal that amorphous SiO_2 preserves much of the ordering present in the crystalline forms on a short or intermediate length scale. For example, the coordination of atoms and the first and second nearest neighbor distances are very similar in the amorphous and crystalline forms, suggesting that both materials have similar building blocks. It is therefore instructive to start our review with the various crystalline allotropes.

The pertinent forms of SiO_2 are α- and β-quartz, tridymite, coesite and stishovite; their thermodynamic stability ranges are indicated in figure 1 and the structural properties are listed on Table 1[3].

The basic bonding unit for all these forms of silica except stishovite is the SiO_4 tetrahedron shown in figure 2(a). Each silicon is surrounded by four oxygen atoms with the Si-O distance ranging from 0.152 nm to 0.169 nm; the tetrahedral O-Si-O bond angle is 109.18^o, the latter being shown in figure 2(b). Each oxygen is bonded to two silicon atoms, with the

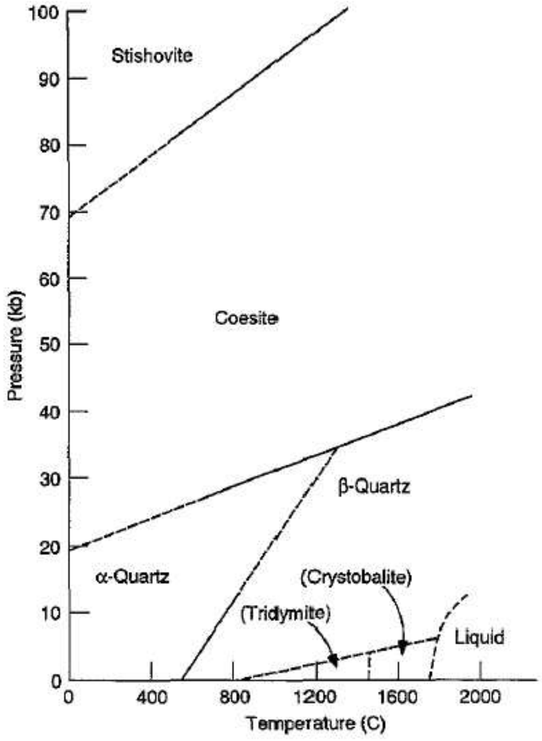

Figure 1: Phase diagram of SiO_2, adapted from[3].

Si-O-Si bond angle varying from 120^o to 180^o, depending on the material.

All forms of silica are constructed from the corner-sharing tetrahedra, such as the SiO_4 building block of figure 2. High-temperature cristobalite and tridymite possess the largest bond angles, and have the most open structures of the crystalline forms of SiO_2. The smaller the bond angle, the denser is the possible packing, reflected in measured density variations.

Another important factor is the effective charge on each atom in SiO_2. For completely covalent bonding, the net excess charge on each atom would be zero, corresponding to four valence electrons on each silicon and six valence electrons (including the *s* electrons) on each oxygen. For completely ionic SiO_2, the net excess charge on each oxygen would be -2, and on each silicon, +4. The actual situation is somewhere between. Numerous calculations have been performed to determine the net charge transfer from Si to O in the various silica structures, and they are in agreement that the effective excess charge on O is about one electron per oxygen atom[4, 5, 6]. Moreover, these calculations indicate that this excess

Table 1: Structural properties of various crystalline forms of silica.

Phase [reference]	Symmetry	Cell params. (nm)	Si-O dist. (nm)	O-O dist. (nm)	Bond angle (deg)	Ring size
Low-temp. quartz[11]	Hexagonal	a = 0.49 c=0.540	0.161	0.260-0.267	144	6
High-temp. quartz[11]	Hexagonal	a = 0.501 c=0.547	0.162	0.260	144	6
High-temp. tridymite [10]		a=0.932 b=0.172 c=8.19 $\alpha, \beta, \gamma = 90^o$	0.158-0.162	0.263	140-173	6
High-temp. cristobalite [11]	Cubic	a=0.176	0.158-0.169	0.263	142-180	6
Coesite[11]	Monoclinic	a,b=0.717 c=1.238 $\gamma = 120^o$	0.160-0.163	0.260-0.267	120	4

charge (i.e., the ionicity) increases as the Si-O-Si bond angle increases.

The temperature- and pressure-stability of the various forms of SiO_2 determine which might be present –as microcrystallites– in thermally grown oxide films or silica glass. Figure 1 shows that the most likely form is tridymite, which is stable at low pressure up to 1470 ^{o}C. High-temperature quartz might not be expected in a typical thermal oxide, as it transforms to tridymite at 870 ^{o}C. However, due to the large stresses possible during oxidation, the high-temperature quartz form and its associated bonding configuration should not be ruled out entirely. Similarly, both low-temperature quartz and coesite should be considered.

Amorphous SiO_2

Two models exist to describe the structure of amorphous SiO_2, the continuous random network model first proposed by Zachariasen[7]) and the microcrystalline model of Randall[8]. In the continuous random network model, the local structural unit (SiO_4 tetrahedron) remains unchanged, with each tetrahedron corner shared with another tetrahedron, as in the crystalline forms. However, the Si-O-Si bond angle will vary from one tetrahedron corner to another, yielding a "continuous random network". In the microcrystalline model,

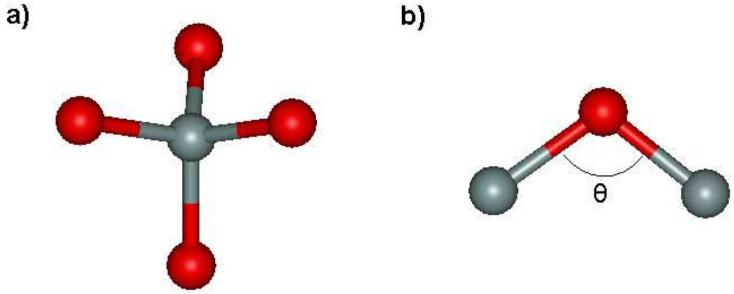

Figure 2: (a) SiO_4 structural unit of most forms of SiO_2, showing tetrahedral coordination. (b) Si_2O bonding configuration with Si-O-Si bond angle θ varying from 120^o to 180^o depending on the form of SiO_2.

the SiO_2 is constructed from microcrystallites of the various allotropic forms of crystalline SiO_2 or alternatively, sub-unit-cell-sized crystallites of one form of SiO_2. In the limit of small crystallites, the two models converge.

The local structure of bulk vitreous silica has been determined by both x-ray and neutron diffraction[1, 2, 9]. These studies are consistent with both the above models, giving Si-O to be 0.16 nm; O-O 0.262 nm; and Si-Si 0.313 nm; all are distances quite close to what is expected for crystalline SiO_2. The difference from the crystalline forms is due primarily to the range in Si-O-Si bond angles present in the vitreous form. A plot of the bond angle distribution obtained by x-ray is shown in figure 3 [1, 10, 11], together with high-temperature tridymite and cristobalite. The latter has two reported bond angles 180^o and 137^o; tridymite has a distribution from 130^o to 175^o because of its large unit cell that contains 330 SiO_2 units. In vitreous silica, the bond angles vary from 120^o to 180^o, with a mean of 152^o[2].

One cannot easily choose between these two main models, as they are both consistent with the best available experimental data. For example, in an idealized random network, one would construct vitreous silica using SiO_4 tetrahedra with the proviso that no two tetrahedra could interpenetrate. The following rules would apply. (1) There would be a random spatial distribution of bond angles, as shown in figure 3. (2) No broken bonds are present. The first problem with this scheme is that rule (2) tacitly implies added spatial correlations in bond-angle distribution not contained in rule (1). For one, the two Si-O-Si bond angles in an Si_3O_{10}, three-tetrahedron unit would not necessarily be a random distribution, but would

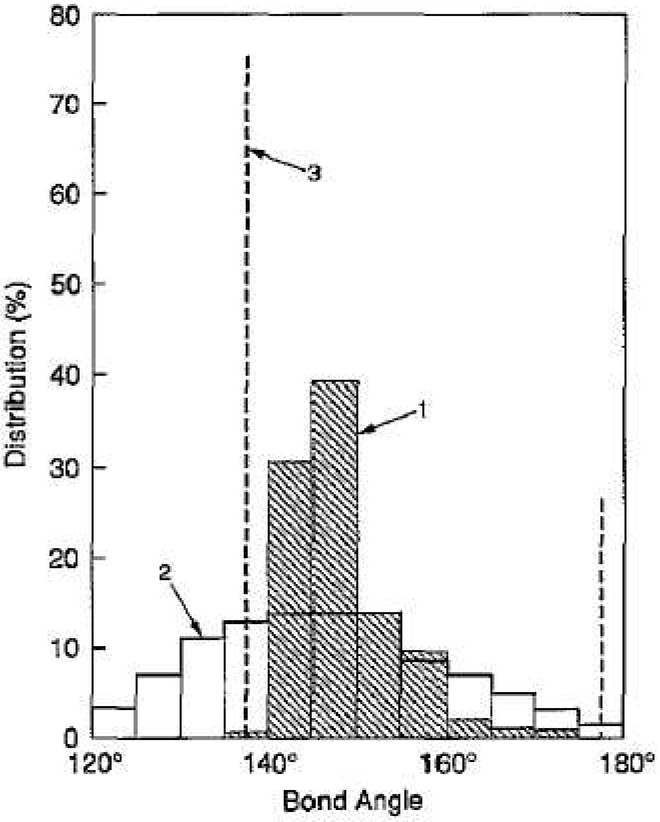

Figure 3: Si-O-Si bond angle distributions (1) tridymite[10]; (2) vitreous silica[1]; (3) cristobalite[11].

be correlated. This is the reason why amorphous SiO_2 would still have some order on the short scale even if one starts modelling its structure as a continuous random network of SiO_4 tetrahedra.

On the other hand, one might construct a model of vitreous silica from grains of coesite, tridymite, and crystobalite to obtain the bond-angle distribution of figure 3. The constituent microcrystalline grains are assumed to be larger than a unit cell dimension, but small enough that Bragg diffraction lines are not distinguished. The connective regions between grains would provide additional freedom in the choice of bond angles. In accord with the notions of the original microcrystalline model, no crystallites smaller than a unit cell would be included. This latter seems to be too stringent a limitation, since tridymite - the crystalline polymorph that most nearly resembles vitreous silica - has a very large unit cell (tridymite is triclinic with $a = 10\mathring{A}$ $b = 17\mathring{A}$ $c = 82\mathring{A}$ and the unit cell contains 330 SiO_2 units[12]).

The true structure of vitreous SiO_2 embraces aspects of both models. There are clearly regions of 10 to 20 atoms in which there exists a correlation in the Si-O-Si bond angles. Such a correlation resembles those found in crystalline forms of silica.

Defects in the perfect structure

There is some ambiguty in defining the concept of a defect in an amorphous material. In crystals, where long range order is present that defines "perfection", any deviation from this long range order may be considered as a defect. In amorphous materials, the concepts one usually encounters in crystals (e.g., vacancies, interstitials or dislocations) are ill defined because the distance between neighboring atoms or the angle subtended by any two pairs of atoms does not have to follow any order. Amorphous SiO_2 is, however, a *network solid*, meaning that it comprises a network of Si-O *chains* and *rings*. This structural peculiarity is a result of the fact that the constituent atoms preserve their coordination and juxtaposition; i.e., every Si atom is 4-fold coordianted and every O atom is 2-fold coordinated and Si atoms always connect to oxygens and vice versa. In terms of disruptions in this coordination and ordering one can define intrinsic defects in amorphous SiO_2.

The existence of a stringent ordering in Si-O chains (i.e., the fact that every Si has to be followed by an O and every O has to be followed by a Si) allows an unambigous definition of an oxygen vacancy. If an O atom is missing from an Si-O chain, the two neighboring Si atoms may undergo some relaxation and produce a (usually strained) Si-Si bond, or at least one of the silicons may relax behind the plane of its three remaining oxygen neighbors and bind to a network oxygen or silicon atom (puckering). As opposed to oxygen vacancies, a silicon vacancy would create four dangling oxygen orbitals resulting in a much greater relaxation of the amorphous network as observed in amorphous silicon[13]. The existence of four reactive orbitals in a small volume region would lead to the formation of e.g., peroxy linkages and thus to the restoration of the ring and chain structure of the glass, although with a deviation from the correct stochiometry.

The above definition of a defect is, however, still not perfect. Namely, the density of Si-O rings and chains is assumed to vary only within certain limits. Large interstitial voids may be constructed, preserving the coordination and ordering of the atoms, yielding a structure that is still consistent with the above picture. The distribution of void sizes depends on the distribution of Si-O-Si angles, but it was suggested that large voids exceeding even 1 nm in diameter[14] may occur in thermal SiO_2. The dominant void size of amorphous SiO_2 is 0.6 nm in diameter[15], but it is completely arbitrary at what point does one consider a large void a “defect”. The lower density of vitreous silica as compared to crystalline forms might well be due to an increased concentration of such larger voids. For SiO_2 films, the number and distribution of such voids depends on the time, temperature and ambient conditions in the growth process. The density of thermal silica films has been shown to vary with these conditions[16]. Some interpretation of such effects has been based on the postulated presence of the several allotropes of crystalline silica, combined microscopically in regions of 20 atoms or so. Voids may well be part of the explanation of several hydrogen- or water-related phenomena in thermal films of silica.

Defects associated with broken bonds

Defects that are associated with a deviation from the normal Si and O coordination involve atoms with broken or dangling bonds. These defects usually introduce dangling orbitals populated by only one (unpaired) electron. Electron spin resonance (ESR) is the tool of choice for study of these centers. There have been reported an impressive array of paramagnetic point defects in the bulk SiO_2 structure, most of which are closely related to various defects in quartz or vitreous SiO_2[17, 18]. A number of these defects have significant electrical properties; indeed, about half of the electrical defects in the Si-SiO_2 system have been shown to be paramagnetic in one state or another.

The most important paramagnetic defects are the following:

The excess-oxygen center, called non-bridging-oxygen (NBO) center, i.e., $O_3 \equiv$Si-O·, and the peroxy radical ($O_3 \equiv$Si-O-O·) are important centers, occurring frequently in bulk fused silica. They do not occur in quartz, since they would require a severe local distortion of the lattice. They have been observed in thin thermal oxides, and seem to behave more or less like those in fused SiO_2.

The essential element of the very important E' center is the moiety $O_3 \equiv Si\cdot$[18], i.e., a dangling Si sp^3 orbital with an unpaired electron in it. The center is usually associated with an oxygen vacancy which gives reason for the dangling Si bond. Altogether, more than 10 E'-like centers have been differentiated in crystalline quartz, in amorphous fused silica, and in thin film silica. A major subdivision is the presence or absence of a complementary adjacent moiety $O_3 \equiv Si^+$. Lesser variations include the presence of ancillary atoms, mainly O or H; numerous variations are summarized in a paper by Warren[17].

Among the various kinds of the E' centers in a-SiO_2, the E'_γ center appears to be the most common high-energy radiation-induced oxygen vacancy center generated in oxides prepared under a variety of conditions. The center also exists in crystalline SiO_2, where it is denoted by E'_1. Extensive experimental[19] and theoretical studies[20, 21] have identified this center as a pair of silicon atoms, one bearing an unpaired electron spin and the other bearing a positive charge, adjoining an oxygen vacancy site ($Si^{\uparrow}$–Si^+). The unpaired electron is localized primarily on an sp^3 bonding orbital of a tetrahedral Si. The positively charged Si atom is far removed from its tetrahedral counterpart and believed to be bonded to a triply coordinated O atom or a five-fold coordinated silicon atom in the oxide network. From the point of view of the ESR experiment, the important feature of this center is that the unpaired electron spin is localized on a single Si atom. The precursor defect is an oxygen vacancy or a Si-Si bond.

The E'_δ center has the same precursor, but a slightly different ESR signature and annealing behavior. These differences result from its different microscopic structure: the positively charged Si is not relaxed back to another network O or Si atom, but stays close to its nearest neighbor Si. As a result, this center is less stable and can be neutralized more easily[21].

The E'_d center comprises a Si atom containing the unpaired spin and an adjacent NBO center. It has been observed primarily in plasma enhanced chemical vapor deposited (PECVD) or plastically densified oxides. It is assumed that the defect is created from rupturing strained Si-O-Si bonds[22, 23].

The E'_s center is observed on the surface of SiO_2 or in ion-sputter deposited oxides.

Contrary to the previous E' centers it is neutral in the ESR active state and invisible for ESR if positively charged[24].

The E'$_\alpha$ center is believed to be a normal $O_3\equiv$Si-O-Si$\equiv O_3$ moiety in a-SiO$_2$, from which the central oxygen is displaced by a radiation event, leaving behind $O_3\equiv$Si-...-Si$\equiv O_3$. This defect is observed to anneal at low temperatures (130 K), which may mean that the displaced oxygen is near (probably in an adjacent peroxy bond) and readily falls back into its place[25].

The E'$_\beta$ center has been observed in high OH-containing x-ray irradiated fused silica[25]. Its counterpart in α-quartz is the E'$_4$ center.

The E'$_{74}$ center received its name from the 74 G doublet observed in the ESR spectrum of x-ray or γ-irradiated high-OH containing fused silica and thin films. The doublet results from a hyperfine interaction with the nearby H atom[26]. Strictly speaking, this center is not an E' center, since it is connected only to two oxygen atoms instead of three. Similarly, the nomenclature for the E'$_{10}$ center is derived from the observed 10.4 G doublet in the above oxides. The doublet is believed to originate from an unpaired spin on a Si atom interacting with an O atom connected to a hydrogen[26].

Diamagnetic defects

Diamagnetic defects are usually detected by mapping out their energy levels in the SiO$_2$ band gap. This is possible by optical absorption/luminescence measurements or studying the charge trapping/detrapping on a defect by, e.g., photoionization. In the charged state these defects are also ESR active.

One of the most important diamagnetic defects is the neutral oxygen vacancy or strained Si-Si bond, since it forms the precursor defect for E'$_\gamma$ and E'$_\delta$ centers. The twofold coordinated Si atom has two dangling bonds with electrons containing opposite spins, making it invisible for EPR measurements. This center was shown to act as a hole trap in SiO$_2$[27]. The peroxy linkage is a common defect in O implanted oxides. An other class of diamagnetic centers contain hydrogen passivated dangling orbitals. These centers may act as possible sources of protons released by radiation interacting with these defects[28]. Examples include the hydrogen passivated Si or O dangling orbital (Si-H, Si-OH) ar the double hydrogen bridge

(Si-H ... H-Si).

Interstitial water and oxygen molecules

Water molecules versus silanol groups

Free molecular H_2O apparently exists in amorphous bulk SiO_2 only if present in quite large concentration, or if there are pore spaces larger than the usual interatomic voids, and on condition of suitable pretreatment. Most of the water is normally bound as silanol ($O_3 \equiv$Si-OH). These silanols may be either isolated and standing alone, or situated adjacent to one or more other silanols. If two silanols are immediately adjacent, they are termed vicinal. A pair of such vicinal silanols represents the siutation of a chemisorbed H_2O molecule in silica. Heating between 100 and 500 ^{o}C eventually liberates the H_2O from the two OH, and the remanent oxygen reforms a bonding bridge between the former host silicons. In contrast, isolated silanols are very difficult to dislodge, requiring temperatures of 900 ^{o}C; and then they liberate H atoms instead of the entire OH group.

If wet silica is desiccated above 500 ^{o}C, it is quite difficult to re-instill silanols by infusion of H_2O at lower temperatures. Some higher temperature or growth process is required to incorporate silanols, even though they are a persistent feature of silica prepared in several different ways. One might expect re-entering H_2O to attack preferentially any siloxane (Si=O=Si) linkages, which represent a distorted and perhaps vulnerable bonding configuration in SiO_2; but there have been no studies touching on this possibility. Excess molecular H_2O has been found to attach to isolated or vicinal silanols, forming physisorbed H_2O. Such water may be easily removed at temperatures of about 100 ^{o}C. Interestingly, a second tier of H_2O molecules adsorbed onto the first physisorbed tier has a higher binding energy than the first tier[29]. This implies that clusters of non-adsorbed H_2O would be viable entities in SiO_2, perhaps in a variable equilibrium with the physi- or chemisorbed H_2O. In all, the disposition of water in silica remains somewhat ambiguous, despite the numerous studies.

The in- and out-diffusion of H_2O in the temperature range above 500 ^{o}C indicates that some molecular recombination and dissociation are part of the processes, since the infusion is proportional to the square root of the overlying vapour pressure. The following reaction has been proposed[30]:

$$H_2O + \equiv \text{Si-O-Si} \equiv \leftrightharpoons \equiv \text{Si-OH...HO-Si} \equiv \quad (1)$$

Migration of H_2O is, however, supposed to take place in the molecular form with the diffusion coefficient:

$$D = 4 \cdot 10^{-7} \exp(-0.76eV/kT) \quad (2)$$

These parameters for vitreous SiO_2 fit thin film thermal SiO_2 quite well in the case of high-temperature diffusion studies[31], and as an element in the kinetics of thin-oxide film growth by steam oxidation[32]. The anneal of radiation-induced defects in both vitreous[19] and thermal[33] silica at low temperature is also well fit. The apparent lower diffusion barrier observed at low temperatures is due to the fact that the silanol formation reaction did not reach equilibrium in those experiments[34, 35].

Interstitial oxygen molecules

Interstitial oxygen molecules can be detected by the characteristic photoluminescence band of O_2 at 1272.2 nm if the oxygen is excited into its characteristic absorption band at 765 nm[36]. The typical interstitial O_2 concentrations vary between $\sim 10^{14}$ to $\sim 10^{18}$ cm^{-1}. Radiation usually increases the interstitial O_2 concentration.

The diffusion barrier for O_2 interstitials was experimentally found to be between 0.7 and 1.6 eV[37] depending on the way the oxide was prepared. In thermal oxides, the Deal-Grove data give 1.2 eV[32]. From these experiments it was concluded that the diffusion barrier is very sensitive to the oxide structure, especially to the distribution of voids.

Spectroscopic properties of defects

Electron paramagnetic resonance has provided so far most of the structural information on defects in amorphous SiO_2. While being of prime importance for applications of fused silica (e.g., for the writing of Bragg gratings) the optical activity of defects usually only had a secondary role as a tool for defect structure studies. The amount of information derived directly from optical methods is limited in most cases by electron-phonon interaction and by inhomogenous broadening effects due to the glassy state. Yet, important information can be extracted about the electronic structure (e.g., position of energy levels) of defects using optical absorption / photoluminescence spectroscopy or photoionization.

The amorphous state influences the optical spectrum of defects in two major ways not encountered in crystals: inhomogenous broadening and cross-correlation effects.

Due to electron-phonon coupling, optical spectra consist generally of broad bands, rather than of separate sharp lines. Since this 'broadening' is a property of each single center and it repeats exactly the same way ('homogeneously') in every other instance of this defect in a crystal, it is called homogeneous broadening. In a non-ideal crystal or, to a greater extent, in glass, the site-to-site non-equivalence of different instances of the same defect causes the optical transition energies to differ. This site-to-site variation results in an additional 'inhomogeneous' broadening of the spectra.

The presence of disorder can give rise to anomalous correlations between different properties of a defect center. A defect center embedded in an ideal crystal can be described by some set of arbitrarily chosen variables, e.g., peak energies of optical bands, luminescence quantum yield, excited state lifetimes, absorption cross-sections and so on. Because of the site-to-site fluctuations, a similar center in glass must be described instead by a probability distribution function of the above variables. It is tacitly assumed that these probability distributions are independent; i.e., disorder-induced site-to-site fluctuations of one variable do not automatically cause functionally correlated changes in another. In practice, however, the fluctuations of different properties of a defect are mutually cross-correlated, for example, oscillator strength, excited state lifetime and transition energy, transition energy and the efficiency of photochemical transformations, components of g-matrix in EPR spectra between themselves and with excited state energies[38]. These phenomena are called cross-correlation effects.

We give here the major reported optical absorption and luminescence bands of defects in non-doped synthetic silica are depicted in figure 4 relying on the published values of their peak positions and halfwidths (full width at half maximum (FWHM)), assuming Gaussian

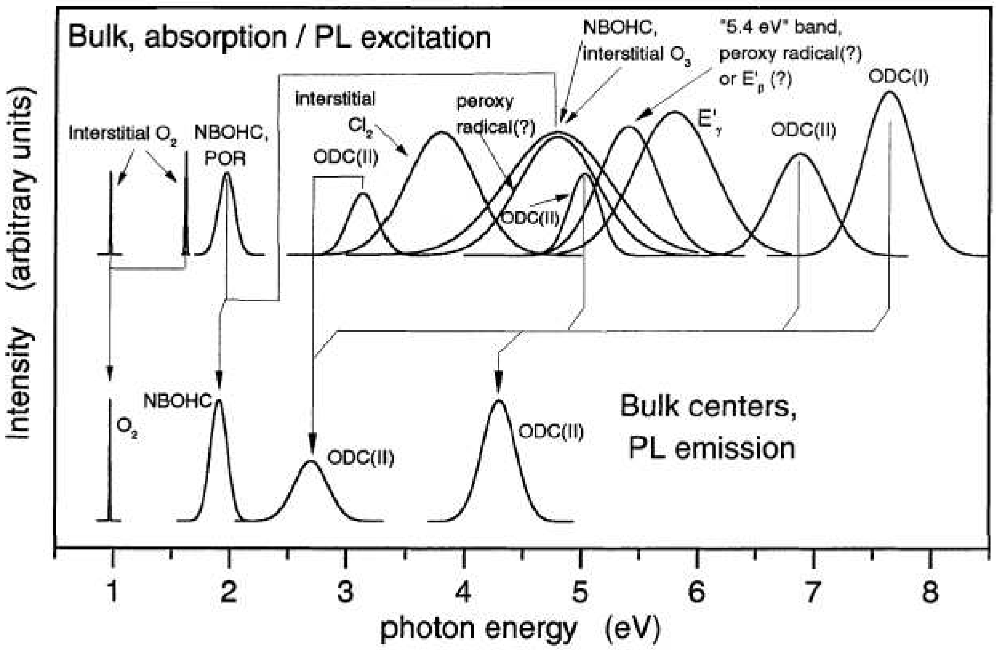

Figure 4: Overview of the major optical excitation and emission bands of defect centers in synthetic silica. The relationship between the emission and excitation bands is indicated. The band intensities shown are arbitrary, the positions and halfwidths correspond to their respective reported values[39].

shape. The intensities of these bands depend on the oxide manufacturing process, irradiation conditions and subsequent treatment. The actual optical spectrum of amorphous SiO_2 is a superposition of these bands with the appropriate intensities.

The reported band parameters are summarized in Table 2. The assignment of the bands is still controversial in some cases.

Table 2: Characteristics of the major optically active defects in bulk silica

Commonly used defect name(s) or acronym(s)	Peak positions of the optical absorption/excitation bands (eV)	Halfwidth (eV) at T=293 K	Oscillator strength f or abs. cross section σ (cm^{-2})	Peaks of PL bands (eV)/ decay constant	EPR signal
E'$_\alpha$, E'$_\beta$, E'$_\gamma$	5.7-5.8	0.8	$f = 0.4$	Not observed	$g_{iso} = 2.0010$
E'$_\delta$ (triplet)	5.0			4.4	$g_{iso} = 2.0020$
					split = 134 G
oxygen vacancy	6.8-7.0	0.4	$f = 0.1 - 0.3$		diamagnetic
oxygen divacancy	4.95-5.05	0.3	$f = 0.15$	4.3-4.4/4 ns	
dicoordinated silicon	3.15	0.34	$f = 1.6 \cdot 10^{-7}$	2.7-2.8/10.2 ms	
Si-Si bond	7.6	0.5	$\sigma = 7.5 \cdot 10^{-17}$ cm^2	4.3-4.4/4 ns	diamagnetic
E'$_{74}$	4.6-6.0	0.6		not observed	$g_{iso} = 2.001$
					split = 74 G
Non-bridging oxygen	4.8	1.05	$f = 0.2$	1.85-1.95/	$g_1 = 2.001$
center (NBOHC)	2.0	0.18	$f = 4 \cdot 10^{-4}$	$(10 - 20)\mu$s	$g_2 = 2.0095$
					$g_3 \approx 2.08$
Peroxy radical	1.97	0.175	$f = 5.7 \cdot 10^{-4}$	not observed	$g_1 = 2.0018$
(POR)	4.8	0.8	$\sigma \approx 5 \cdot 10^{-18}$		$g_2 = 2.0078$
	≈ 7.6	0.65	0.65($\pm$50%)		$g_3 \approx 2.067$
Interstitial O_2	edge$\approx$ 7 eV	continuum	$\sigma = 10^{-19}$ cm^2		Triplet ground
	1.62	0.012	$f = 10^{-8} - 3 \cdot 10^{-10}$	0.975	state
	0.975	0.011	$f = 1.2 \cdot 10^{-8}$	0.975/0.8 s	
Interstitial O_3	4.8	1.0	$\sigma = 5 \cdot 10^{-18}$ cm^2	0.975	diamagnetic
peroxy linkage	3.8	0.7	$\sigma = 10^{-19}$	not observed	diamagnetic

CHAPTER III

THEORETICAL APPROACH

Two methods currently exist which model the solid state from first principles, using only the atomic numbers and coordinates as input. Their key difference lies with the property which is used as the variational parameter in order to minimize the system energy. In Hartree-Fock (HF) theory, the electronic wavefunctions take on this role whereas density functional theory (DFT) uses the charge density. The advantages of DFT over HF for modeling defects in semiconductors and insulators arise from its lower computational demands and better scaling and its inclusion of the electron correlation. In HF on the other hand, the wavefunctions are mathematically meaningful as opposed to DFT where the wavefunctions do not necessarily have physical significance. In practice however, the wavefunctions calculated in DFT often bear a strong resemblance to experiment.

This chapter is intended to outline both the theoretical background of density functional and pseudopotential theory and implementation details specific to VASP (Vienna Ab-initio Simulation Package). VASP is a self-consistent density functional code applied to supercells. The majority of the results discussed in this thesis have been produced using this method.

In the first section we describe the basics of density functional theory leading to the Kohn-Sham equations that allows one, in principle, to map exactly the problem of a strongly interacting electron gas (in the presence of the nuclei) onto that of a single particle moving in an effective non-local potential. The solution to the Kohn-Sham equations requires the use of approximations for the exchange-correlation energy of an electronic system. Here we briefly describe and compare the local density approximation and the generalized gradient approximation.

Subsequently, pseudopotential theory is outlined, that allows one to replace the strong electron-ion potential with a much weaker "pseudopotential" that describes all the salient features of a valence electron moving through the solid.

Periodic calculations, based on the plane wave expansion of the electronic wavefunctions have the benefit that electronic bands (Bloch states) can be reproduced in a solid. We use periodic repetitions of a supercell to mimic the properties of an amorphous or crystalline solid. The application of supercells, Bloch's theorem and k-point sampling allows one to expand the electronic wavefunctions in a finite set of plane waves.

In the final section we introduce the molecular dynamics procedure based on the calculation of the Hellmann-Feynmann forces. The derived equations of motion determine the relaxation of the ions in the supercell towards the minimum energy configuration.

Density functional theory

DFT finds its formal justification in the Hohenberg-Kohn theorem[40], which in its original form is applicable to the ground state of a system of spinless particles in an external potential. The theorem may be summarized as follows:

The ground-state energy of a system of identical spinless particles is a unique functional of the particle density. (The ground state is assumed to be nondegenerate).

This functional has its minimum value for the correct ground-state density, when particle-number conserving variations of the electron density are considered.

The ground-state energy functional is written as:

$$E[n] = \int v_{ext}(\mathbf{r})n(\mathbf{r})d\mathbf{r} + F[n] \tag{3}$$

where v_{ext} is the external potential, i.e., the potential determined by the positions of the nuclei. The central and remarkable feature of the theorem is that there is a one-to-one correspondence between the electron density $n(\mathbf{r})$ and the external potential. The fact that the external potential determines the density is obvious, the converse, however, is surprising and initially was greeted with some scepticism.

The functional $F[n]$ includes all kinetic energy and electron-electron interaction terms. It is convenient to split off from $F[n]$ the energy due to the Coulomb-interaction, also called Hartree-energy[1]:

---

[1] e is the charge of the electron and ϵ_0 is the electric permittivity of vacuum

$$F[n] = \frac{e^2}{8\pi\epsilon_0}\int\int \frac{n(\mathbf{r})n(\mathbf{r}')}{|\mathbf{r}-\mathbf{r}'|}d\mathbf{r}d\mathbf{r}' + G[n] \tag{4}$$

The exact form of $G[n]$ is unknown. The ground state of the system is formally obtained by minimizing $E[n]$ with respect to density variations that conserve the number of particles N:

$$\int n(\mathbf{r})d\mathbf{r} = N \tag{5}$$

This leads to the variational equation:

$$\delta\left\{E[n] - \mu\int n(\mathbf{r})d\mathbf{r}\right\} = 0 \tag{6}$$

in which a Lagrange multiplier μ is introduced due to the constraint 5. Applying 3 4 and 6 the ground state determining equation is found:

$$v_{ext}(\mathbf{r}) + \frac{e^2}{4\pi\epsilon_0}\int \frac{n(\mathbf{r}')}{|\mathbf{r}-\mathbf{r}'|}d\mathbf{r}' + \frac{\delta G[n]}{\delta n(\mathbf{r})} = \mu \tag{7}$$

where the last term on the left hand side is the functional derivative of $G[n]$ with respect to $n(\mathbf{r})$. Even if the functional form of $G[n]$ were known, eq. 7 would still not give us a procedure to actually calculate the correct $n(\mathbf{r})$. Kohn and Sham[41] however supply a procedure that results in one-particle equations (the so-called Kohn-Sham (KS) equations) that we do know how to solve. Their line of reasoning runs as follows: consider a system of N non-interacting electrons in some external potential $v_{ext,s}(\mathbf{r})$. The ground-state density of this system is called n($\mathbf{r}$). The functional $F[n]$ in 4 reduces to $T_s[n]$, the kinetic energy functional of non-interacting electrons, and the equation determining $n(\mathbf{r})$ is given by:

$$v_{ext,s}(\mathbf{r}) + \frac{\delta T_s[n]}{\delta n(\mathbf{r})} = \mu_s \tag{8}$$

The general form of $T_s[n]$ is again unknown but now there is an alternative way to obtain $n(\mathbf{r})$: for non-interacting electrons the many-particle ground-state wave function is simply a completely antisymmetrized product of one-electron wave functions $\phi_i(\mathbf{r})$ (Slater determinant), each of which obeys the Schrödinger equation:

$$\left\{\frac{-\hbar^2}{2m}\nabla^2 + v_{ext,s}(\mathbf{r})\right\}\phi_i(\mathbf{r}) = \epsilon_i\phi_i(\mathbf{r}), i = 1...N, \tag{9}$$

where m denotes the electron mass. The prescription is to select those N states $\phi_i(\mathbf{r})$ that have lowest energy ϵ_i. The density for this system of electrons is then given by:

$$n(\mathbf{r}) = \sum_{i=1}^{N} |\phi_i(\mathbf{r})|^2 \tag{10}$$

So for this particular system of non-interacting electrons there is indeed a way of finding the solution to 8. Kohn and Sham now show that this procedure may be used in the case of *interacting* electrons as well. The functional $G[n]$ is split up into two terms:

$$G[n] = T_s[n] + E_{xc}[n] \tag{11}$$

in which $T_s[n]$ is the kinetice energy of a system of non-interacting electrons with a density $n(\mathbf{r})$ and in which the remaining term $E_{xc}[n]$ *by definition* is called the exchange and correlation energy of the interacting system with density $n(\mathbf{r})$. Equation 7 now becomes:

$$v_{ext}(\mathbf{r}) + \frac{e^2}{4\pi\epsilon_0}\int \frac{n(\mathbf{r}')}{|\mathbf{r}-\mathbf{r}'|}d\mathbf{r}' + \frac{\delta E_{xc}[n]}{\delta n(\mathbf{r})} + \frac{\delta T_s[n]}{\delta n(\mathbf{r})} = \mu \tag{12}$$

This equation has the form of 8; the only difference is that $v_{ext,s}(\mathbf{r})$ is replaced by an "effective" potential $v_{eff}[n]$:

$$v_{eff}[n] = v_{ext}(\mathbf{r}) + \frac{e^2}{4\pi\epsilon_0}\int \frac{n(\mathbf{r}')}{|\mathbf{r}-\mathbf{r}'|}d\mathbf{r}' + \frac{\delta E_{xc}[n]}{\delta n(\mathbf{r})} \tag{13}$$

By analogy with the non-interacting case, the correct ground-state density of the interacting system is found by the self-consistent solution of the following set of one-particle equations (KS-equations):

$$\left\{\frac{-\hbar^2}{2m}\nabla^2 + v_{eff}(\mathbf{r})\right\}\psi_i(\mathbf{r}) = \epsilon_i\psi_i(\mathbf{r}), i = 1...N \tag{14}$$

$$n(\mathbf{r}) = \sum_{i=1}^{N} |\psi_i(\mathbf{r})|^2 \tag{15}$$

Note that the self-consistency requirement is caused by the functional dependence of $v_{eff}[n]$ on $n(\mathbf{r})$. The total ground-state energy of the electron system is then given by:

$$E[n] = T_s[n] + \int v_{ext}(\mathbf{r})n(\mathbf{r})d\mathbf{r} + \frac{e^2}{8\pi\epsilon_0}\int\int\frac{n(\mathbf{r})n(\mathbf{r}')}{|\mathbf{r}-\mathbf{r}'|}d\mathbf{r}d\mathbf{r}' + E_{xc}[n] \tag{16}$$

We have:

$$T_s[n] = \sum_{i=1}^{N}\int \psi_i^*(\mathbf{r})\left(\frac{-\hbar^2}{2m}\nabla^2\right)\psi_i(\mathbf{r})d(\mathbf{r}) \tag{17}$$

In order to find the self-consistent solution to 15 and to calculate $E[n]$ it is necessary to adopt some explicit form for $E_{xc}[n]$. A very useful approximation has proven to be:

$$E_{xc}[n] = \int \epsilon_{xc}(n(\mathbf{r}))n(\mathbf{r})d(\mathbf{r}) \tag{18}$$

where ϵ_{xc} is the exchange and correlation energy of an interacting electron gas with uniform density n. This is called the local density approximation (LDA), since the exchange and correlation energy at position $\mathbf{r}$ is assumed to depend on the density at point $\mathbf{r}$ only. This assumption is valid if $n(\mathbf{r})$ is constant. The approximation can be considered acceptable for electron systems with almost constant or slowly varying $n(\mathbf{r})$. The approximation is not justified for systems with large density gradients such as semiconductors. The apparent success of LDA in such cases is even more remarkable if one notes that, because of the definition implied in 11, $E_{xc}[n]$ must also contain some kinetic energy contribution apart from the "real" exchange and correlation energy contribution as in 18; this is because $T_s[n]$ represents only a part of the kinetic energy of the *interacting* system. By "real" exchange and correlation energy we mean the remaining energy of an electron gas when the kinetic and Hartree energies (and the energy due to a possible external potential) have been substracted from the total energy. In the view of the successful application of 18, the latter feature is either of minor importance or its effect is washed out by adopting approximate forms for ϵ_{xc}.

An improvement in the approximation of the exchange and correlation energy of the inhomogenous system is achieved with the inclusion of density-gradient corrections in E_{xc}[42] (this is called the generalized gradient approximation (GGA)):

$$E_{xc}^{GGA}[n] = \int f(n(\mathbf{r}), \nabla(n(\mathbf{r})))d(\mathbf{r}) \tag{19}$$

where f contains a parametrized analytic function fit to a particular system.

The superiority of the GGA with respect to LDA is not clear in the applications to solids. Sometimes GGA reproduces the experimental phenomena; in other cases the GGA overcorrects the LDA results. The general trend in the applications to solids of the these functionals is that the GGA underestimates the bulk modulus and zone center transverse optical phonon frequency of the solid[43, 44], corrects the binding energy[45, 44] and corrects or overcorrects the lattice constants compared to LDA[43, 46]. For example, the correct ferromagnetic bcc ground structure for iron[47, 48] and the correct energy difference between α-quartz and stishovite in SiO_2 system[49] were predicted by GGA functionals. Other studies also suggested that GGA might be more suitable for the study of SiO_2 systems[50, 52].

Pseudopotential Theory

It is a well known fact in chemistry that the properties of a molecule depend predominantly on the valence electrons and hardly at all on the core electrons. Core electrons occupy inner, inert, shells of atoms. Their main role is to shield the outer electrons–valence electrons–from the nuclei. It is therefore tempting to eliminate them from an electronic structure calculation, replacing them instead by an effective potential acting only on valence electrons.

Due to the requirement of orthogonality between core and valence states, the wavefunctions of the valence electrons vary rapidly in the core region, as these always have a small spatial extent. Obviously, if the core electrons are removed, this constraint disappears. This suggests replacing the true valence wavefunctions by a pseudo-wavefunction varying smoothly near the nucleus (see Figure 5).

In order to eliminate the core states and replace the valence-electron wavefunction by a pseudo-wavefunction, we write

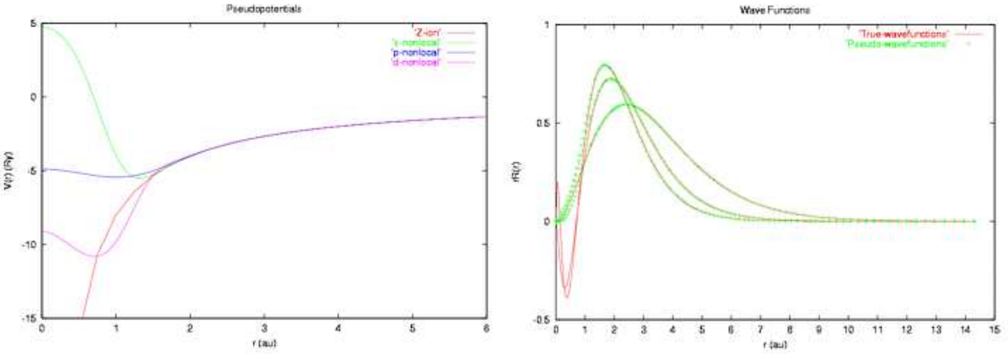

Figure 5: a) Comparison of the true ionic potential of Si (red curve) and the angular momentum dependent components of the pseudopotential. b) Comparison of psuedowavefunctions and the real wavefunction

$$|\phi_v\rangle = |\psi_v\rangle + \sum_c \beta_c |\psi_c\rangle \text{ with } \beta_c = \langle\psi_c|\phi_v\rangle \tag{20}$$

since $\langle\psi_c|\psi_v\rangle = 0$. Here $|\psi_c\rangle$ and $|\psi_v\rangle$ are the real core and valence electron wavefunctions, respectively, and $|\phi_v\rangle$ is the pseudo-wavefunction replacing $|\psi_v\rangle$. In this way, the rapid variations in the near-core region, contained in $|\psi_v\rangle$, can be cancelled out.

It is now convenient to define a projection operator which projects any state onto the core states[53]:

$$\hat{P} = \sum_{c'} |\psi_{c'}\rangle\langle\psi_{c'}| \tag{21}$$

satisfying $(1 - \hat{P})|\psi_c\rangle = 0$, and more importantly

$$(1 - \hat{P})|\phi_c\rangle = \psi_v\rangle \tag{22}$$

The energy eigenvalue equation satisfied by a valence-band state is

$$\hat{T}|\psi_v\rangle + \hat{V}(\mathbf{r})|\psi_v\rangle = E\psi_v\rangle. \tag{23}$$

This equation is also satisfied by the core states, $|\psi_c\rangle$, with the same potential $V(\mathbf{r})$. Bringing in 21 and 22, this equation can be rewritten as

$$(\hat{T} + \hat{V}^{ps})|\phi_v\rangle = E\phi_v\rangle \tag{24}$$

with $\hat{V}^{ps}$ the pseudopotential given by

$$\hat{V}^{ps} = \hat{V}(\mathbf{r}) + \sum_{c'}(E - E_{c'})|\phi_c\rangle\langle\phi_{c'}| \tag{25}$$

This pseudo-Schrödinger equation, known as a pseudopotential equation, provides the same eigenvalues as the original Schrödinger equation 23 but the core levels are missing. Despite this achievement, this equation is still not perfect: $\hat{V}^{ps}$ involves a nonlocal operator, $\hat{P}$ as well as the eigenvalue we are trying to find. From 22, we have

$$\langle\phi_v|\phi_v\rangle - \langle\psi_{c'}|\hat{P}|\psi_{c'}\rangle = \langle\psi_v|\psi_v\rangle \tag{26}$$

which reveals another weakness in this simple theory: if the pseudo-wavefunction is normalised then the true wavefunction is not. The difference between the true density and the pseudo charge density is termed an orthogonalisation hole and is a consequence of the non-locality of $\hat{V}^{ps}$.

Performing calculations with nodeless pseudo-wavefunctions instead of the rapidly varying true wavefunctions would seem advantageous; however, reliable pseudopotentials are relatively complex. Applying these seems useful only if they can be transferred from one system to another, i.e., from a single atom to an atom in a molecule or solid, which implies that the core states must be considered frozen. These are not supposed to change in different chemical environment.

There are two ways of determining pseudopotentials: either by means of model potentials, or through ab initio techniques.

Traditionally, empirical pseudopotentials constructed by using some experimental data have been adopted[54]. These empirical pseudopotentials, however, have a weak point that the charge density does not coincide with that of the real atom even outside the core region ($r > r_c$).

Ab initio pseudopotentials

The majority of the pseudopotentials currently used in electronic-structure calculations are generated from all-electron atomic calculations. Within the density function theory, this is done by assuming a spherical screening approximation and solving the radial Kohn-Sham equation

$$\left[-\frac{1}{2}\frac{d^2}{dr^2}+\frac{l(l+1)}{2r^2}+V(n(r))\right]\psi_{nl}(r)=E_{nl}\psi_{nl}(r) \tag{27}$$

where

$$V(n(r))=-\frac{Z}{r}+V^H(n(r))+V_{xc}^{LDA}(n(r)) \tag{28}$$

with $n(r)$ the sum of the electron densities for the occupied wavefunctions $\psi_{nl}(r)=rR_l(r)$; l defining the quantum state. This method has been extented to include GGA corrections[55, 56].

Most pseudopotentials are constructed such that they satisfy four general conditions[57, 58, 59, 51, 60]:

1. The generated valence pseudo-wavefunction generated from the pseudopotential should be nodeless;

2. Norm conservation: The normalised radial pseudo-wavefunction, $\psi_l^{ps}(r)$ is equal to the normalised all-electron wavefunction, $\psi_l^t(r)$, beyond a chosen cut-off radius r_c[59]:

$$R_l^{ps}(r)|_{r=r_c}=R_l^t(r)|_{r=r_c}\text{with}r>r_c \tag{29}$$

or converges rapidly to that value (we have omitted the principal quantum number n for simplicity);

3. In the core region ($r<r_c$) the charge density associated with the two wavefunctions should be equal[58]

$$\int_0^{r_c} r^2|R_l^{ps}(r)|^2dr=\int_0^{r_c} r^2|R_l^t(r)|^2dr \tag{30}$$

This restriction may pose a serious problem when expanding the total energy using a plane-wave basis. This is the case of first-row transition metals characterised by localised d-electrons. Some attempts have been made to generate smooth pseudopotentials using a plane-wave set[61, 62]. Vanderbilt[63], and independently Blöchl[65], dropping the norm-conservation condition, were able to overcome this difficulty. Using lower kinetic energy cut-offs for the plane-wave expansion, these authors introduced the so-called (ultra)soft-pseudopotentials.

4. The all-electron and pseudo valence eigenvalues are identical for a particular atomic configuration, i.e., $E_{ps} = E_t$;

If a given pseudopotential meets all the above conditions, it is commonly referred to as an ab initio pseudopotential.

Once the pseudo-wavefunction is obtained, the screened pseudoptential can be recovered by inverting the radial Schrödinger equation 27:

$$V_l^{ps} = E_l - \frac{l(l+1)}{2r^2} + \frac{1}{2rR_l^{ps}(r)}\frac{d^2}{dr^2}[rR_l^{ps}(r)] \tag{31}$$

The pseudopotential concept requires that the scattering properties of the pseudo and all-electron atom are the same for the pseudo-wavefunction at the specific matching radius, i.e., the core radius r_c[58]. This radius controls the overall accuracy and "transferability" of the pseudopotential: the first order energy derivatives of the radial logarithmic derivative of the pseudo- and atomic-wavefunction coincide with each other at r_c.

Projector augmented-wave method

Wavefunctions of real materials have very different signatures in different regions of space: in the bonding region the wavefunction is fairly smooth, whereas close to the nucleus the wavefunction oscillates rapidly due to the large attractive potential of the nucleus. This is the source of the difficulty of electronic structure methods to describe the bonding region to a high degree of accuracy while accounting for the large variations in the atom center. The strategy of the augmented-wave methods has been to divide the wavefunction into parts, namely, a partial-wave expansion within the atom centered sphere and an envelope function outside the sphere. The envelope function is expanded into plane waves or some other convenient basis set. Envelope function and partial-wave expansions are then matched with value and derivative at the sphere radius.

At the root of the projector augmented-wave (PAW) method, developed by Blöchl [66], is a transformation that maps the valence wavefunctions onto a new Hilbert-space comprising pseudo wavefunctions that are to be identified as the envelope functions. This transformation is linear and the resulting pseudo wavefunctions are computationally easy to handle. This transformation changes the representation of the wavefunctions in a way reminiscent of the change from the Schrödinger to the Heisenberg picture. A transformation T back from the pseudo wavefunctions $|\Psi\rangle$ to the one-electron Kohn-Sham (KS) wavefunctions $|\Phi\rangle$ may be determined[66], and one can obtain physical quantities (e.g., total energies), represented as the expactation value $\langle A\rangle$ of some operator A from the pseudo wavefunctions either directly as $\langle\Phi|A|\Phi\rangle$ after transformation to the KS wavefunctions $|\Phi\rangle = T|\Psi\rangle$ or as the expectation value $\langle A\rangle = \langle\Psi|A'|\Psi\rangle$ of an operator $A' = TAT$ in the Hilbert space of the pseudo wavefunctions.

The benefits of the PAW method over pseudopotential methods are the following:

Firstly all errors can be systematically controlled so that there are no transferability errors. A pseudopotential constructed from an isolated atom is not guaranteed to be accurate for a molecule. In contrast, the converged results of the PAW method do not depend on a reference system such as an isolated atom, because it uses the full density and potential.

The PAW method provides access to the full charge and spin density, which is relevant for hyperfine parameters. Hyperfine parameters are sensitive probes of the electron density near the nucleus. In many situations they are the only information available that allows to deduce atomic structure and chemical environment of an atom.

The plane wave convergence is more rapid than in norm-conserving pseudopotentials and should in principle be equivalent to that of ultra-soft pseudopotentials. Compared to the ultra-soft pseudopotentials, however, the PAW method has the advantage that the total energy expression is less complex and therefore is expected to be more efficient. The construction of pseudopotentials requires one to determine a number of parameters. As they influence the results, their choice is critical. Also the PAW method provides some flexibility in the choice of pseudo wavefunctions. However, this choice does not influence the converged results.

The supercell approach

The supercell approach models periodic systems of atoms. The boundary conditions imposed ensure a periodic charge density which constrains the Kohn-Sham orbitals to satisfy Bloch's theorem.

The usual approach adopted within supercell formalisms is to expand both the Kohn-Sham orbitals and the electronic wavefunctions in plane waves. This choice is natural because of the inherent periodicity of the system. The Kohn-Sham orbitals at a point, **k**, in the Brillouin zone are thus expanded:

$$\psi_{nk}(\mathbf{r}) = \sum_{\mathbf{G}} c_{n\mathbf{k}}(\mathbf{G}) \exp[i(\mathbf{k} + \mathbf{G}) \cdot \mathbf{r}] \tag{32}$$

The number of plane waves which are used in the expansion of the wavefunctions is determined by the cut-off energy E_c (usually all plane waves with $G^2/2 < E_c$ are included).

Sampling of the Brillouin zone

The occupied (valence) states at each **k** point contribute to the electronic potential in the bulk solid so that, in principle, an infinite number of calculations are needed to compute this potential. However, the electronic wavefunctions at **k** points that are very close together will be almost identical. Hence it is possible to represent the electronic wavefunctions over a region of **k** space by the wavefunctions at a single **k** point. In this case the electronic states at only a finite number of **k** points are required to calculate the electronic potential and hence determine the total energy of the solid. The charge density is usually sampled at a small set of carefully chosen special k-points. In practice, this approach gives a good approximation to the exact charge density. The special points lie within the irreducible Brillouin zone, i.e., the smallest part of the Brillouin zone which unfolds into the whole zone, when the symmetry operations of the system are employed. In VASP, we employ the method of Monkhorst and

Pack[67] with usually only one **k** point (the L point). This procedure is reasonable because of the large size of our supercells ($> 10^3 \mathring{A}$), i.e., the small irreducible Brillouin-zone volumes. Convergence in total energy with respect to the number of applied **k** points in SiO_2 systems using similar cell sizes was tested in earlier work[68].

Nonperiodic systems

The Bloch theorem cannot be applied to a system that contains a single defect or to an amorphous solid. A continuous plane-wave set and hence an infinite number of plane waves would be required for a defect calculation in a periodic crystal. Amorphous materials have no periodicity.

To circumvent both problems, we use a large supercell that is locally amorphous, i.e., has the correct a-SiO_2 density, structure factor, Si-O bond length and Si-O-Si angle distribution. The supercell is simple cubic and contains 72 atoms. The physical size is 1 nm x 1 nm x 1 nm (Fig 6). To justify the applicability of this approach for modeling defects in amorphous SiO_2, extensive tests have been carried out in the past to test the convergence of defect total energies with respect to cell size. It was found that the interaction of a defect with its periodic images becomes small (less than about 0.3 eV) for supercells of the above size. This error is comparable to the fluctuations in the total energy of defects resulting from the amorphous state.

Supercells used in our calculations, like the one in Fig. 6, were prepared by the Monte-Carlo bond-switching method[69, 70] that has proved to generate amorphous structures having the proper chemical bonding orientation, density and radial distribution function (this function is characteristic of the pair correlation of atomic positions and bond angle distributions over the amorphous solid). In the Monte-Carlo bond-switching method one starts with a crystalline structure of SiO_2 (usually crystobalite) as an initial configuration. Then two nearest neighbor Si or O atoms are selected randomly (atoms 1 and 5 on Fig. 7). Let two other nearest neighbors to 1 and 5 be 2 and 6 (these have to be distinct from 1 and 5, but can otherwise be randomly selected). The fundamental step of the bond-switching method is to break the two Si-O bonds that connect the oxygens between 1-2 and 5-6 and

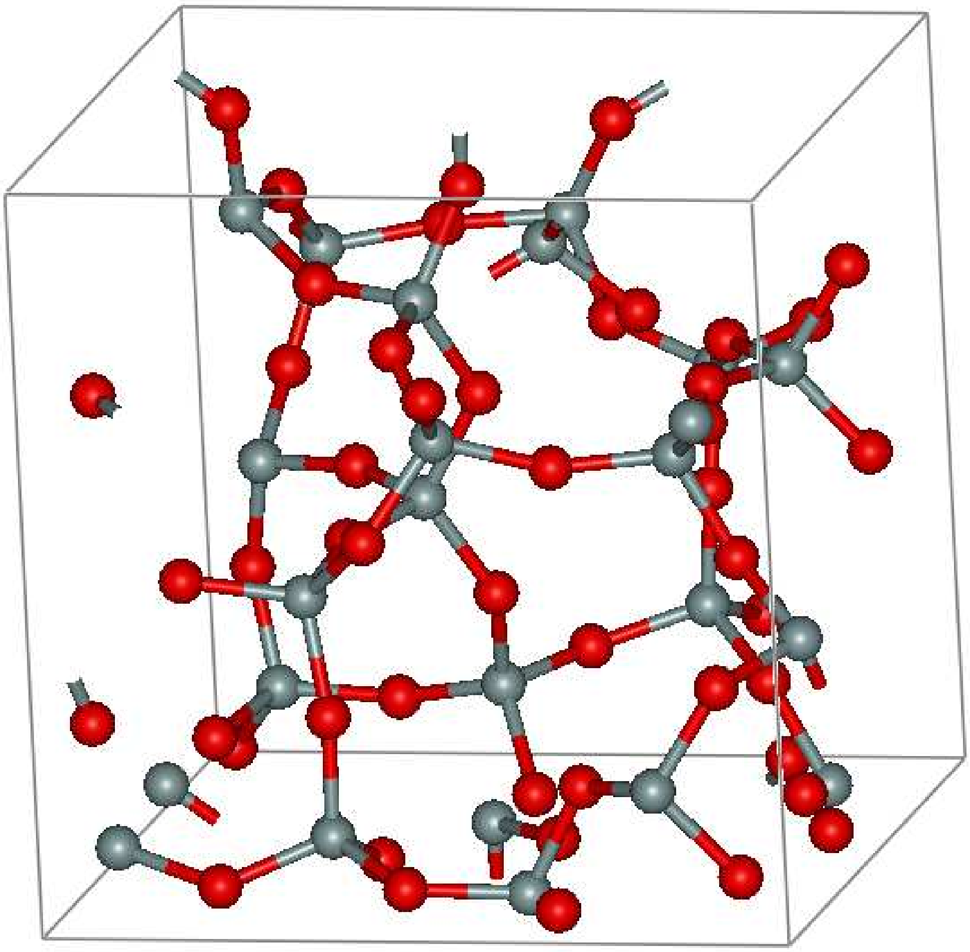

Figure 6: 72-atom amorphous SiO_2 supercell used in the calculations. If the cell is repeated periodically there are no dangling atoms on the surface.

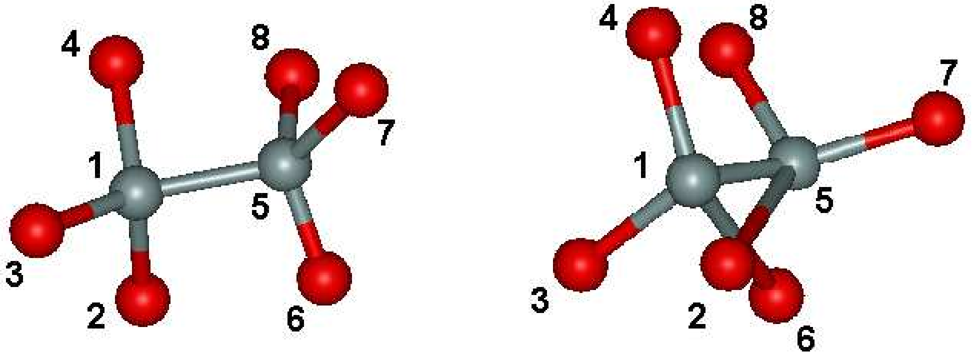

Figure 7: Fundamental step of the bond-switching method

bind them to the opposite silicon, i.e., bind 2 to 5 and 6 to 1. A metropolis algorithm is used to determine if this move is accepted or rejected, i.e., the probability for accepting the new configuration is

$$P = \min[1, \exp(-\Delta E/kT)] \tag{33}$$

where the energy of the system is defined based on the Keating model:

$$E = E(\psi, \{\mathbf{r_i}\}) = \sum_{i,j \in \psi} \frac{1}{2} k_\theta b_0^2 (\cos\theta_{ij} - \cos\theta_0)^2 + \sum_{j \in \psi} \frac{1}{2} k_b (b_j - b_0)^2 \tag{34}$$

where $\{\mathbf{r_i}\}$ are the positions of the atoms and ψ is the set of bonds connecting pairs of atoms, j represents the jth bond with length b_j and angle θ_{ij} between bonds i and j connected to a common atom. b_0 and θ_0 are the bond length and bond angle in crystalline SiO_2 and the k-s are spring constants.

Relaxation of the ionic system

Up to this point the relaxation of the electronic configuration to its ground state has been considered, while the ionic positions and the size and shape of the unit cell have been held fixed. The positions of the ions and the size and shape of the unit cell can be included as dynamical variables in a Lagrangian (usually referred to as "Car-Parinello Lagrangian") and the Euler equations of motion give the necessary equations for the relaxation of the system.

In the Car-Parinello scheme the Kohn-Sham energy functional $E[\{c_{n\mathbf{k}}\}]$ is a function of the set of coefficients of the plane-wave basis set $\{n\mathbf{k}\}$. Each coefficient $n\mathbf{k}$ can be regarded as the coordinate of a classical “particle”. To minimize the KS energy functional, these “particles” are given a kinetic energy, and the system is gradually cooled until the set of coordinates reaches the values $\{n\mathbf{k}\}_0$ that minimize the functional. The Car-Parinello Lagrangian takes the form:

$$L = \sum_i \mu\langle\dot{\psi}|\dot{\psi}\rangle + \sum_j \frac{1}{2}M_j\dot{R}_j^2 + \sum_\nu \frac{1}{2}\beta\dot{\alpha}_\nu^2 - E[\{\psi_i\}, \{\mathbf{R_j}\}, \{\alpha_\nu\}] \tag{35}$$

where μ and β are fictitious masses associated with the electronic wavefunctions $(\psi_i\rangle)$ and coordinates defining the unit cell (α_ν), E is the KS energy functional and R_j is the position of ion j with mass M_j. The kinetic term is due to the fictitious dynamics of the electronic degrees of freedom and the dynamics of the ions and the parameters defining the cell size and shape. The KS energy functional takes the place of the potential energy in a conventional Lagrangian formulation.

Equations of motion

One obtains the following equations of motion for the positions of the ions and the coordinates of the unit cell:

$$M_j\ddot{\mathbf{R}}_\mathbf{j} = -\frac{\delta E}{\delta \mathbf{R_j}} \tag{36}$$

$$\beta\ddot{\alpha}_\nu = -\frac{\delta E}{\delta\alpha_\nu} \tag{37}$$

The equations of motion for the degrees of freedom asociatied with the dynamics of the ions and of the unit cell can be integrated at the same time as the equations of motion for the electronic states and, as will be shown below, provide a method for performing ab-initio dynamical simulations of the ionic system. A relaxation of the ionic system can be performed using these equations simply by removing kinetic energy from the electronic system, the ionic system, and the motion of the unit cell. In this case the system will evolve until the total energy of the system is minimized with respect to all of these degrees of freedom and the ionic configuration will have reached a local energy minimum. However, integration of the equations of motion for the ions and for the unit cell is not as straightforward as it first appears. This is because *physical* ground-state forces on the ions and integrated stresses on the unit cell cannot be calculated for arbitrary electronic configurations, as shown in the following section.

The Hellmann-Feynman theorem

As the ion moves from one position to another, the wave functions must change to the self-consistent KS eigenstates corresponding to the new positions of the ions if the value of the KS energy functional is to remain physically meaningful. These changes contribute to the force on the ion:

$$f_j = -\frac{dE}{d\mathbf{R_j}} = -\frac{\delta E}{\delta \mathbf{R_j}} - \sum_i \frac{\delta E}{\delta \psi_i}\frac{d\psi_i}{d\mathbf{R_j}} - \sum_i \frac{\delta E}{\delta \psi_i^*}\frac{d\psi_i^*}{d\mathbf{R_j}} \tag{38}$$

Comparison to 37 shows that the “force” in the Lagrangian equation of motion is only the partial derivative of the KS energy functional with respect to the position of the ion which is not the *physical* force on the ion, but only the force the ion would experience from a particular electronic configuration. It can be shown, however, that when each electronic wavefunction is an eigenstate of the Hamiltonian the two final terms in 38 sum up to zero[71]. It is only in this case that the partial derivative of the KS energy with respect to the position of the ion gives the *physical* force on the ion. This result is referred to as the Hellmann-Feynman theorem[72, 73]. Each time that the positions of the ions or the size and shape of the unit cell are changed, the electrons must be brought close to the ground state of the new ionic configuration in order to calculate forces and stresses for the new ionic configuration. These calculated forces can then be used to update the ionic positions again.

Calculations using VASP

The results in this thesis were obtained using the Vienna Ab-initio Simulation Package, a parallelized, high-performance software package for performing ab-initio quantum-mechanical molecular dynamics (MD) simulations using pseudopotentials or the projector-augmented wave method and a plane wave basis set[74]. Although this software is capable of performing finite-temperature MD simulations, we have used it only for zero-temperature calculations.

Here is a short summary of some highlights of the VASP code:

1. VASP uses the PAW method or ultra-soft pseudopotentials. Therefore, the size of the basis-set can be kept very small even for transition metals and first row elements like C and O. Generally not more than 100 plane waves (PW) per atom are required to describe bulk materials; in most cases even 50 PW per atom will be sufficient for a reliable description.

2. In any plane wave program, the execution time scales like N^3 for some parts of the code, where N is the number of valence electrons in the system. In the VASP, the prefactors for the cubic parts are almost negligible leading to an efficient scaling with respect to system size. This is made possible by evaluating the non-local contributions to the potentials in real space and by keeping the number of orthogonalisations small.

3. VASP uses a rather "traditional" and "old fashioned" self-consistency cycle to calculate the electronic ground-state. The combination of this scheme with efficient numerical methods leads to an efficient, robust and fast scheme for evaluating the self-consistent solution of the Kohn-Sham functional. The implemented iterative matrix diagonalisation schemes (RMM-DISS, and blocked Davidson) are probably among the fastest schemes currently available.

4. VASP includes a full featured symmetry code which determines the symmetry of arbitrary configurations automatically.

5. The symmetry code is also used to set up the Monkhorst Pack special points allowing an efficient calculation of bulk materials, symmetric clusters. The integration of the band-structure energy over the Brillouin zone is performed with smearing or tetrahedron methods. For the tetrahedron method, Blöchl's corrections, which remove the quadratic error of the linear tetrahedron method, can be used resulting in a fast convergence speed with respect to the number of special points.

For a given supercell geometry, the accuracy of the calculations is determined by the types of pseudopotentials used, cutoff energy and the number of k-points. For dynamical calculations (atomic relaxations) we have used ultrasoft pseudopotentials for all the atoms involved in our supercell (Si, O and H). We have used a cutoff energy of 600 eV and only one k-point (L point) in the irreducible Brillouin-zone. We have considered an atomic geometry as "relaxed" if the force on all atoms was less than $0.1\ \mathrm{eV}/\mathring{A}$ and the difference between successive total energies reduced below 10^{-4} eV.

The formation energy of a defect is defined as the total energy difference of the defect and its precursor (the configuration of the system prior to the reaction that produces the defect). The formation energy is calculated by putting the initial (precursor) and final (defect) reaction products into two supercells and relaxing each cell and taking the difference of the total energies of the relaxed structures.

Energy barriers for reactions or diffusion are more complicated to calculate, since, if complex defects are involved, the phase space of the process is quite large. In all the cases studied in this thesis it was possible to reduce the dimensionality of the phase space to one using approximations or experimental evidence about the intermediate products of a reaction. For every reaction, energy barriers had to be calculated in a unique way, tailored for the particular reaction process. This will be outlined in the chapters where the results are presented. For diffusion, the following procedure was used: The diffusing species was placed into a void and relaxed to equilibrium. Then an immaginary line was drawn connecting one (marked) atom of the diffusing molecule with its periodic image. The coordinate of this atom of the diffusing molecule was put along the imaginary line at several different points and a full relaxation was performed with one coordinate of the marked atom of the diffusing molecule fixed. This reduced the phase space of the diffusion problem to one dimension. It is important to note that, using this method, the diffusing molecule was free to rotate or move in the plane perpendicular to the diffusion trajectory.

Vibrational frequencies of the Si-O bonds in the non-bridging oxygen, silanol and (5)Si-OH- defects were determined by calculating the spring constant k of the Si-O bond in these complexes. The spring constant was calculated using the total energy of a "frozen" system (i.e., with all atoms fixed) where the O atom along the Si-O line was displaced by $\pm 0.1\mathring{A}$ from its equilibrium position. The total energy between this configuration and the ground state relates to the spring constant:

$$E - E_0 = \frac{kA^2}{2} \text{ with } A = 0.1\mathring{A} \tag{39}$$

The $0.1\mathring{A}$ displacement approximately corresponds to the amplitude of zero-point oscillations of the Si-O bond in the NBO. In these cases the accuracy of electronic and MD calculations had to reach 10^{-6} eV to obtain a more accurate ground state.

For the study of optical phenomena, excited states had to be generated. These were created by manually fixing the band occupancy numbers (i.e., an electron had to be forced to occupy an energy band higher than its ground state). For calculating optical matrix elements PAW potentials were necessary, since the matrix elements include a complicated extra correction term related to the nonlocal pseudopotential operator in the pseudopotential case and only in the all-electron case does this extra term vanish.

We have calculated the optical matrix elements for transitions from different valence levels (Ψ_b) to the (uniquely defined) defect level (Ψ_a) and evaluated the absorption coefficient (averaged over all the possible light polarizations):

$$\alpha(\omega) = \frac{4\pi e^2 \hbar^2}{\epsilon_0 m^2 \omega^2} \sum_i | < \Psi_a | \nabla | \Psi_b > |^2 \delta(\omega + E_a - E_b) \tag{40}$$

In practical calculations δ-functions are replaced by Lorentzians with $\gamma = 0.2$ eV.

CHAPTER IV

REACTIONS AND DYNAMICS OF WATER AND OXYGEN MOLECULES IN BULK SiO_2

Introduction

The presence of H_2O and O_2 molecules is known to affect the nature and the density of defects that form during SiO_2 glass synthesis, thermal oxidation of silicon, irradiation of SiO_2 or subsequent mechanical or thermal treatment. As a result, water incorporation into silica glass reduces the viscosity, index of refraction, acoustic velocity and density of the glass, while it causes an increase in the thermal expansion coefficient and crystallization rate[75, 76]. Additional water diffusion into silica glass also reduces the static fatigue life [79] and accelerates structural modification of the glass[77]. If water molecules are present in the oxidation ambient, the rate of silicon oxidation also increases[32].

Despite the wide interest in the behavior of O_2 and H_2O molecules in bulk SiO_2, the understanding of the atomic scale processes remains limited. For example, water molecules are known to form silanol (Si-OH) groups in the oxide, but the relative concentration of silanol to interstitial water depends on the way the oxide was manufactured and subsequently treated, raising questions about the most stable form of water in the oxide. Exposure of SiO_2 to water vapour results in the appearance of various OH vibrational bands (SiOH, hydrogen bonded OH, H_2O, hydrogen bonded water), the Si-H band[78] and also in a shift of the SiO_2 structural bands[77]. There is also significant oxygen exchange between H_2O and SiO_2 over the entire volume of the oxide as shown by ^{18}O tagged water diffusion experiments[80]. These data suggest that water is highly reactive, while other experiments (e.g., on the analysis of water diffusion [35]) provide evidence that it also exists as an interstitial molecule in the oxide.

Oxygen molecules are more inert than H_2O in bulk SiO_2, i.e., they are less likely to form defects that alter the properties of the oxide. The presence of interstitial (i.e., intact) O_2 molecules in thin films grown in oxygen was observed by infrared photoluminescence[36].

The main interest in studying the behavior of O_2 molecules in SiO_2 is due to its role in the silicon oxidation process. Thus most of the work was focused on the reactions of O_2 at the Si-SiO_2 interface.

Reactions of O_2 molecules with the SiO_2 structure were observed at the vacuum-SiO_2 and the Si-SiO_2 interfaces in thin films grown in ^{16}O and subsequently exposed to $^{18}O_2$[81]. The ^{18}O-^{16}O exchange was found to be small in between the film surfaces, although the film thickness in these experiments did not exceed 80 $\AA$[82]. To explain this behavior it was suggested based on ab-initio calculations that the oxygen molecule might break up into two O atoms that diffuse in an atomic form via peroxy (Si-O-O-Si) linkages[50]. Another possibility for the O_2–SiO_2 reaction is the formation of an ozonic bond (Si-O-O-O-Si)[83]. The existence of interstitial ozone (O_3) molecules was confirmed by the photostimulated phosphorescence of excited O_2 molecules created by the UV dissociation of interstitial O_3[84]; however, the results may be applicable for the UV dissociation of the ozonic bond as well.

Besides the reactions of H_2O and O_2 with the perfect amorphous SiO_2 network, several other reactions may take place at defect sites. For example, infrared measurements confirm that water molecules react with dangling Si bonds created by neutron irradiation[85]. The concentration of charged oxygen vacancies (E' centers) in irradiated oxides was suggested to decrease due to their reaction with interstitial O_2 and H_2O molecules[86].

As it has been indicated above, the behavior of water and oxygen in amorphous bulk SiO_2 is very versatile and not devoid of controversies. In this chapter we attempt to provide a systematic first-principles study of the various defect formation mechanisms between interstitial O_2 and H_2O molecules and the amorphous SiO_2 network. In particular, we investigate the possible defects that may form also taking into account the different possible charge states. We provide the formation energies and geometrical structure of these defects and map out the most probable defect formation scenarios. For the reactions with the lowest formation energy ($H_2O + SiO_2 \leftrightharpoons 2$ SiOH, $2\ H_2O \leftrightharpoons OH^- + H_3O^+$, $O_2 + SiO_2 \leftrightharpoons$ Si-O-O-O-Si), we calculate the reaction barrier and –in some cases– the variation of the formation energy within the amorphous medium.

After proving that the most stable form of both H_2O and O_2 is the interstitial molecule, we calculate their diffusion barrier in the oxide. We find that variations in the local bonding of the amorphous network result in a much wider range of phenomena than one normally encounters in crystals. For example, diffusion of H_2O is possible through six-member and larger rings with small energy barrier (~0.8 eV), but it is very unlikely in smaller rings, where the barrier is much higher. On the other hand, when in a diffusion dead-end, an H_2O molecule is more likely to break up at an O atom site, resulting in two silanol groups. In turn, an H_2O molecule can reform on the other side, allowing diffusion by a novel and unusual "reactive cut" through the network. In general, however, the lowest energy reaction is to form stable silanol groups. As opposed to water, oxygen molecules are more inert and do not react with the network. They diffuse as interstitial molecules with an energy barrier that is very sensitive to the local ring topology.

We also explain the difference in the E' center generation rates, dependant on the oxide manufacturing process, by investigating the reactions between H_2O and O_2 interstitials and charged and neutral oxygen vacancies. While both interstitials annihilate the E' defects in an exothermic reaction, by calculating the activation barriers we show that irradiated wet oxides (e.g., Suprasil-1 with $[OH] \geq 10^{19} cm^{-3}$) are more likely to have more E' centers than dry oxides (e.g., Suprasil-W1 with $[OH] \leq 5 \cdot 10^{16} cm^{-3}$) as it has been found experimentally[86, 87]. Neutral vacancies are, however, annihilated by a higher energy barrier which is why these oxides may have the same amount of precursors prior to irradiation.

Equilibrium positions of H_2O and O_2 interstitials

Amorphous SiO_2 can be viewed as a material having interconnecting voids of different sizes that are bordered by Si-O rings. We have studied the properties of H_2O and O_2 interstitials in voids that are $\approx 6 \mathring{A}$ in diameter, which corresponds to the average intrinsic void size in vitrious SiO_2, as estimated by positronium lifetime measurements[15]. These voids are surrounded mainly by 6-member Si-O rings, which is the dominant ring size in SiO_2[88].

We have found that both H_2O and O_2 molecules have an equilibrium position in the middle of the voids of the SiO_2 network. In the case of O_2 molecules, the total energy has a

Table 3: Total energy (in eV) of interstitial H_2O and O_2 molecules in voids of different sizes. We used the total energies in a $6\mathring{A}$ void as the reference point.

void diameter	H_2O energy	O_2 energy
$\sim 7.0\mathring{A}$	-0.2	-0.2
$\sim 6.0\mathring{A}$	0	0
$\sim 5.0\mathring{A}$	1.2	1.5
$\sim 4.5\mathring{A}$	1.9	4.0
$\sim 4.0\mathring{A}$	2.2	4.2

global minimum in the middle of the void with no local minima (metastable configurations) elsewhere, whereas for H_2O molecules there are additional interstitial configurations with a local minimum in the total energy. In these metastable interstitial configurations the oxygen of the water molecule is attracted to a network Si atom (typical Si-O distance is $1.87\mathring{A}$ where the O is in the H_2O molecule) and the hydrogens orient themselves in such a way that they are about 1.9-$2.0\mathring{A}$ away from the oxygens adjacent to the network Si atom (Fig. 8a). The reason for the existence of these metastable configurations is that Si atoms in SiO_2 are somewhat positively charged, thus they attract the negative (oxygen) end of the H_2O dipole molecule, whereas oxygens tend to collect most of the negative charge therefore they attract the positive H atoms of the H_2O molecule. Such configurations of interstitial water have been suggested by infrared measurements based on the shifts in the vibrational frequency of the O-H bond[78]. The total energy difference between the various metastable configurations and the middle-of-the-void configuration did not exceed 0.2 eV.

A large variation in total energies can be found, however, if we place the O_2 and H_2O interstitials into voids of different sizes in the oxide (Table 3). The data show, that the total energy increases rapidly if the void diameter decreases below $\approx 6\mathring{A}$, however, it is practically constant in larger voids. Therefore, in thermal equilibrium, the H_2O and O_2 interstitials are most likely to reside in voids that are $6\mathring{A}$ or larger, possibly because in these voids they can be far enough (at least $2\mathring{A}$ away) from network atoms so that the interaction between the interstitial molecules and the network becomes small.

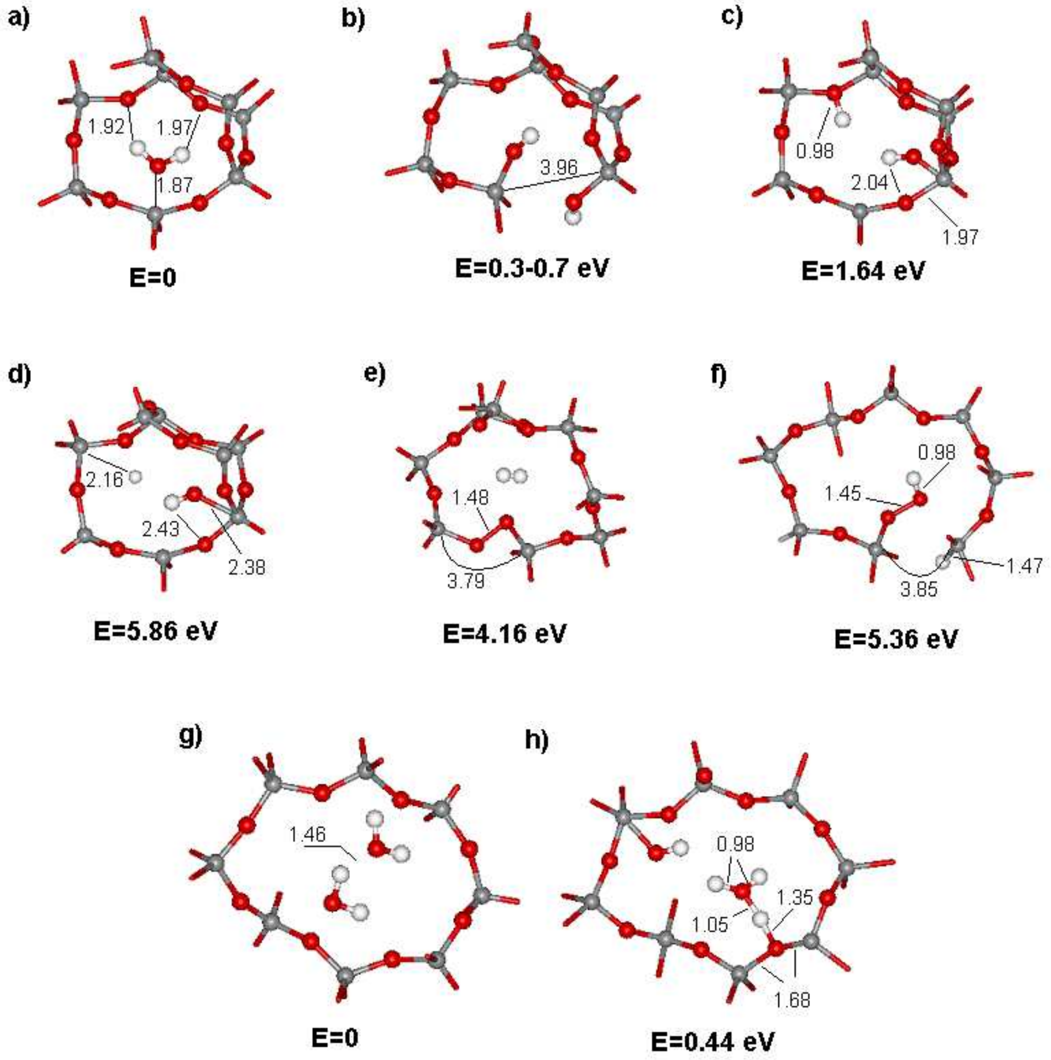

Figure 8: Possible reactions of H_2O and the defect-free SiO_2 network. a) Initial configuration of a H_2O molecule in a void bordered by a 6-member ring as a part of the supercell. b) vicinal silanol groups. The energy range shows the site-dependence of the formation energies. c) H^+ and OH^- bound to network O and Si atoms. d) neutral H and OH weakly bound to network O and Si atoms. e) Peroxy (Si-O-O-Si) linkage and interstitial H_2 molecule. f) H-terminated peroxy radical (Si-O-O-H) and Si-H. g) Two water molecules in a bigger (8-member) ring. f) H_3O^+ and OH^- bound to network O and Si atoms.

Reactions between water and the defect-free SiO_2 network

In Fig. 8 we show the formation energies and relaxed geometries of several defects that may form as a result of a reaction between interstitial H_2O molecules and the defect-free SiO_2 network. The starting point is always an H_2O molecule in a metastable equilibrium position $1.87\mathring{A}$ away from a network Si atom (Fig. 8a) in a $6\mathring{A}$ void. The formation energy of the final reaction products depends on the local electronic environment in an amorphous solid. Here we have arbitrarily chosen a Si-O-Si segment of the 6-member Si-O ring bordering the void that was replaced by the final defect complexes. The distribution of Si-O-Si angles and Si-O bond lengths in this ring is $130 - 170^o$ and 1.62-1.66 $\mathring{A}$, respectively, corresponding to typical values in a-SiO_2. The absence of large deviations from the average values means that there are no regions of extreme stress in this particular ring, therefore the formation energies calculated at different sites of this ring should be similar. We have calculated this site-dependence only for one reaction ($H_2O + SiO_2 \leftrightharpoons 2\ SiOH$) and found that the extremal values of the formation energies differed by only 0.2 eV for the 6-member ring shown on Fig. 8. This result is in contrast to a variation of 0.4 eV if the formation energies are calculated in different rings.

Stability of various charged species

Certain defects, which may be created by the radiation induced splitting of H_2O and O_2 interstitials, are highly reactive radicals and will react with the network in a barrierless reaction. For example, UV irradiation may split a water molecule into H and OH or H^+ and OH^-[89]. All of these species bind to the network to some extent. H and H^+ were found to bind to network oxygens by 0.2[90] and 1.65 eV[52], while our calculations show that OH and OH^- are bound to network Si atoms by ~0.3 eV in both cases. Similarly, interstitial O atoms are also not stable[50] and immediately form peroxy linkages. Negatively charged oxygen complexes bind to network silica[91].

A further, important question is the stability of the reaction products with respect to their charge state. Generally, a defect level would be empty above the Fermi level and filled below it. In bulk SiO_2, unlike e.g., in doped semiconductors, the position of the Fermi-level is uncertain, because usual defect concentrations are too small to pin the Fermi level, thus different charge states may coexist.

By comparing total energies of different charge states after allowing the charged defect to relax, we have found that OH molecules are more stable in the negative, while H atoms are more stable in the positive charge state in concordance with earlier work[52]. In both cases there are substantial relaxations from the positions of the neutral defect as mentioned earlier. However, this result is only valid if there is a source of electrons/holes for charging the OH/H. The higher stability of OH^- and H^+ versus the neutral species is also consistent with the observation that splitting up H_2O molecules into charged species is favoured by $5.8eV - 1.6eV = 4.2eV$ (cf. Fig. 8c and d). Moreover, H^+ in SiO_2 has been observed, e.g., via the dynamics of of interface trap formation[92], whereas shifts in the OH vibrational bond due to charging were seen in the infrared spectra of SiO_2[93].

In thin films, where neutral hydrogen is unstable versus H^+[52], OH molecules may act as electron traps, i.e., they may immediately capture an electron from the Si valence band. Once an OH molecule is negatively charged, it binds to a Si atom making it 5-fold coordinated. Before capturing an electron, the OH has an energy level about 1.3 eV above the SiO_2 valence band and this level drops below 0.9 eV in the negatively charged state after binding to the Si atom. Based on the location of this energy level, we suggest that neutral OH molecules may be one of the water-related electron traps observed in as-grown SiO_2 films[94].

Formation of adjacent silanols

Based on formation energies, the most likely reaction between an interstitial H_2O and the defect-free SiO_2 network is the formation of two adjacent (vicinal) SiOH groups (see Fig. 8b). By putting the water molecule into different voids and picking different locations for the silanol groups, we found that formation energies vary between 0.3 eV - 0.7 eV, where the lower values are obtained in the 6-8 member rings. The positive formation energies mean that water is most stable as an interstitial molecule, seemingly contradicting the observation that most of the "wet" oxides contain water in the form of silanols[78]. The reason for this may be that, upon the oxidation process, SiOH groups are predominantly formed in the

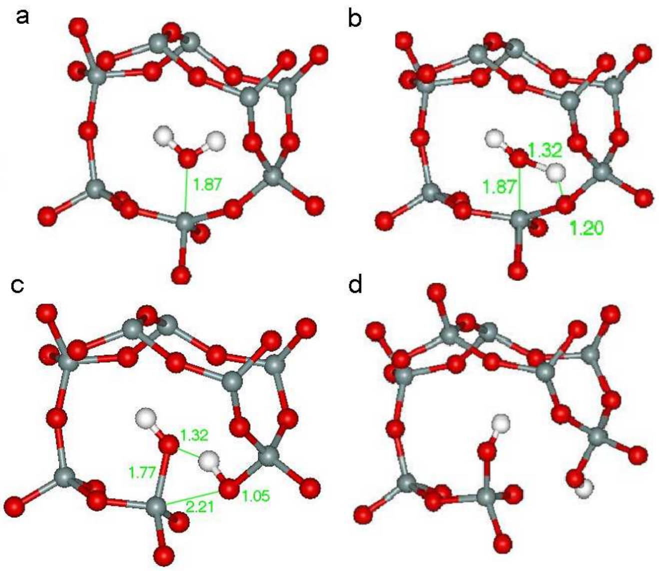

Figure 9: Stages of the $H_2O + SiO_2 \leftrightharpoons 2SiOH$ reaction: a) H_2O initially in the middle of the void; b) H_2O bends and stretches toward a network oxygen; c) breakup occurs (saddle point); d) final configuration: two adjacent SiOH groups. All distances are in Angstroms.

vicinity of the Si/SiO_2 interface that is rich in oxygen vacancies and usually accumulates some stress. Therefore, it is different from the defect-free and unstrained bulk oxide that we have modeled in our calculations. Indeed, H_2O-related vibrational bands appear in the infrared spectra if water is introduced into the bulk oxide at low temperatures[78].

We have calculated the activation barrier for this reaction following the scenario described by the IR observations of Davis and Tomozawa[78] (Fig. 9); the oxygen atom of the water was placed next to a network Si while one of the hydrogen atoms gets attached to one of the oxygen atoms from the network. Simultaneously, the H-O distance for this hydrogen atom in the water molecule increases (the distances between the main participating atoms are also shown in the figure). The configuration shown in Fig. 9c corresponds to the saddle point of the reaction.

Figure 8 shows the reaction energies (the total energy differences between the final and initial products of reaction) for different possible reactions between H_2O and SiO_2. It is clear that the final product with the lowest energy is two silanol groups (Fig. 8b). The range

0.3–0.7 eV corresponds to different local environments. The reaction barrier is 1.5 eV, but, because of the large variation of the energy of the H_2O molecule in the network, there is a corresponding variation in the reaction barriers as well.

Reactions resulting in the formation of other defects

The reaction with the next lowest formation energy is the splitting of H_2O into H^+ and OH^- (Fig. 8c). Right after the reaction both the OH^- and H^+ are interstitials, however they relax to the network and bind to Si and O atoms respectively. The total energy difference between the interstitial H_2O and the relaxed reaction products is 1.6 eV; however, right after the H_2O split, while the OH^- and H^+ is interstitial, the total energy of the products is higher. We can calculate this energy and use it as a lower estimate for the energy barrier of this reaction.

We found that the binding energy for OH^- is only 0.3 eV; this much energy is required to move the molecule into the middle of the $6\mathring{A}$ void from its relaxed position only $1.8\mathring{A}$ away from a network Si atom. For H^+ the binding energy was found to be 1.65 eV[52]. Therefore, right after the H_2O is split, the total energy of the interstitial OH^- and H^+ complex can be estimated to be 1.6 eV + 0.3 eV + 1.65 eV = 3.55 eV. The actual barrier is probably higher, but for our purposes it suffices to note that this energy is already too high to be overcome in a thermally activated process. Therefore, we assume that this reaction channel may only be open in oxides exposed to radiation. Indeed, UV radiation is known to split water molecules[89], and neutron irradiation releases hydrogen in the oxide. One possible source of this hydrogen may be the interstitial H_2O molecule[92].

Subsequent reactions have formation energies exceeding 4 eV (Fig. 8 d,e,f), therefore we did not calculate reaction barriers or site-dependent formation energy variations in these cases. Because of the high energy of the reaction products, these reactions are unlikely in defect-free oxides.

Reaction between two H_2O interstitials in a cavity in amorphous SiO_2

Water molecules may cluster in the bigger voids of the oxide[95], i.e., form hydrogen-bonded complexes with each other and network O atoms. In such cases two H_2O molecules may react with each other forming OH^- and H_3O^+ only at a cost of 0.44 eV (Fig. 8f).

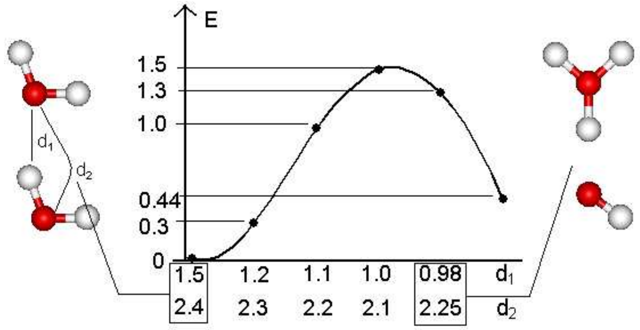

Figure 10: Energy barrier of the 2 $H_2O \leftrightharpoons H_3O^+ + OH^-$ reaction. At left is the initial configuration as in Fig. 8g. The total energies were obtained by fixing d_1 at different values and relaxing the entire supercell at each value. The final reaction products (H_3O^+ and OH^-) are to the right.

In this calculation, we put two water molecules into the biggest void in our supercell (Fig. 8g). The O-H distance between the two molecules was initially $1.46\AA$. The small distance means that they were "squeezed" together by the surrounding solid even prior to the reaction. (As a comparison, the bond length of hydrogen bonding in ice is $1.8\AA$.) We found that, by putting two H_2O molecules into one void (like the one on Fig. 8g), the total energy increases by 0.8 eV. To calculate the reaction barrier we approximated the O atom of the first H_2O molecule to the H atom of the second by keeping them fixed and varying the distance d_1 between them (Fig. 10). The supercell was relaxed in each configuration with the above constraint. We have also monitored the distance of the two oxygens (d_2) to ascertain the saddle point of the reaction (in the saddle point d_2 has a minimum). The two water molecules break up into H_3O^+ and OH^- complexes at about $d_1 = 1.0\AA$. The moderate, 1.5 eV barrier means that, if the oxide is exposed to water vapor at high temperatures, then this reaction may contribute to the formation of oxide trapped charges in as-processed SiO_2. The final reaction products will relax and bind to network atoms as seen on Fig. 8f.

Reactions involving O_2

A medium-energy-ion-scattering spectroscopy study[81, 82] has shown evidence for reactions between the O_2 and a-SiO_2 at oxide surfaces. We have investigated two reactions between interstitial O_2 and the defect-free SiO_2 network: the formation of adjacent peroxy linkages and the formation of an ozonyl linkage. Atomic oxygen is unstable as an interstitial; it would form a peroxy linkage in a barrierless reaction.

Our results for the formation energies are consistent with those of Chelikowsky et al.[83], who calculated them for a quartz cluster. We find the formation energy of two peroxy linkages to be 0.92 eV (or 0.46 eV per peroxy unit, Fig. 11b) as opposed to 0.6 eV per peroxy unit in Ref. [83]. The higher value probably occurs because interstitial O_2 introduces less strain in an amorphous material that has larger voids and a more flexible structure; therefore, it has a lower total energy in its initial configuration. We also confirm that an ozonyl linkage has lower energy than the interstitial O_2 molecule in bulk amorphous SiO_2 by 0.23 eV; see Fig. 11c (the result for quartz is 0.3 eV[83]).

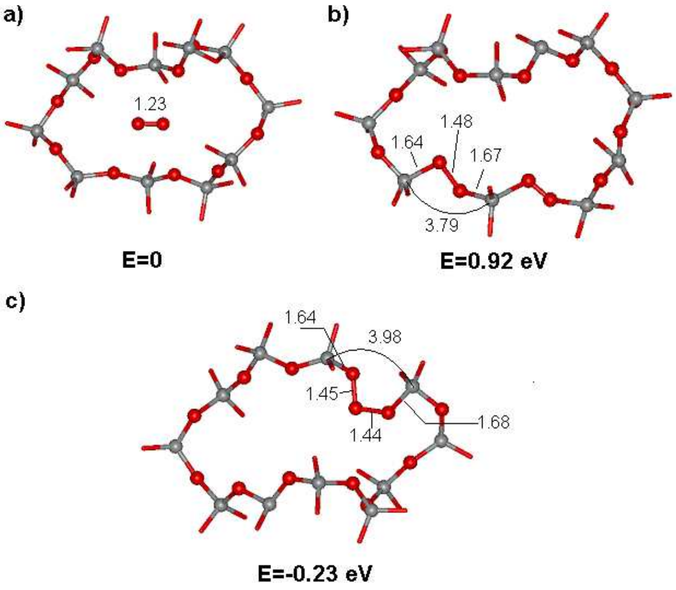

Figure 11: Reactions of O_2 and the defect-free SiO_2 network. a) Initial position of an O_2 molecule in the middle of an 11-member (only $6\mathring{A}$ in diameter) ring. b) Two adjacent peroxy linkages. c) Ozonyl linkage. Notice that the Si-Si distance increases from $3.2\mathring{A}$ to $3.79\mathring{A}$ and $3.98\mathring{A}$ to accomodate the strain, but the Si-O distances remain little changed.

To explain the lack of oxygen exchange in the bulk oxide we have calculated the energy barrier for the formation of ozonyl. In this calculation we approximated one O atom of the interstitial O_2 molecule toward the center of the Si-O bond by varying the distance d on Fig. 12. The oxygen of the O_2 and one network Si atom far away from the defect site were kept fixed while the structures were relaxed at each value of d. The reason for fixing a distant Si was to prevent drift of the supercell as the O_2 is pushed closer to the network. We found that, if d is reduced below $\sim 1.7\AA$ the ozonyl structure becomes more stable.

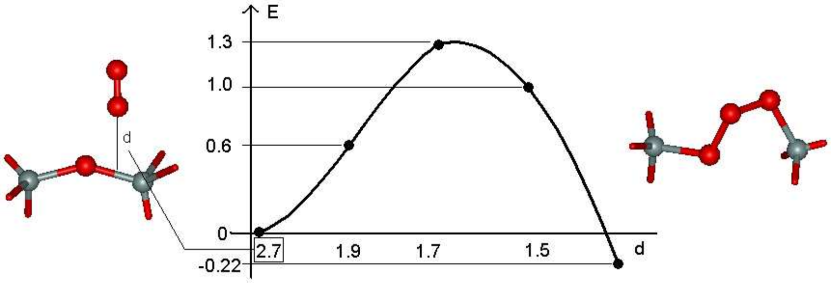

Figure 12: Energy barrier of the O_2 + $SiO_2 \leftrightharpoons$ Si-O-O-O-Si reaction. At left is the initial configuration as in Fig. 11a. The total energies were obtained by fixing d at different values and relaxing the entire supercell at each value. The ozonyl linkage becomes stable below $d =\sim 1.7\AA$.

We have found a $\sim$ 1.3 eV energy barrier for the ozonyl formation that is at the upper end of the diffusion barrier of O_2 in the 6- or higher member rings of the oxide ($\sim 0.6 - 1.5$ eV[96]). We suggest that the relatively large value of this barrier compared to the diffusion barriers is the reason for the lack of O_2 exchange in bulk SiO_2. However, as the O_2 molecule diffuses closer to the Si/SiO_2 interface, the structure of the oxide changes. It has been observed that, besides the increased concentration of various defects, the density of the oxide also increases towards the Si-SiO_2 interface[97]. The increased density results in the dominance of smaller rings where the diffusion barrier was found to be much higher ($>$ 1.5 eV)[96], making the ozonyl formation reaction more favorable. The incorporation energy of a free gas-phase O_2 molecule into SiO_2 was found to be $\sim$ 2 eV[83, 98]. This is the energy barrier the O_2 molecule has to overcome to enter the network of interstitial voids in the oxide. The high incorporation barrier makes the formation of ozonyl linkages also at the

Table 4: H_2O and O_2 diffusion barriers (in eV) as a function of ring size and ring diameter (in $\AA$). For $\sim 6\AA$ and $\sim 4\AA$ rings the variation of the barriers in different rings is included.

ring size	ring diameter	H_2O diffusion barrier	O_2 diffusion barrier
7	7	0.8	0.5
6	6	0.8-0.9	0.6-1.0
5	4.5	1.8	1.9
4	4	2.0-2.2	2.4-2.8

vacuum-SiO_2 surface preferrable. Once ozonyl is formed, the O_2 may reform in a reverse reaction overcoming a barrier of $\sim$ 1.5 eV. Since different O atoms may be incorporated in the reformed O_2 molecule, the ozonyl formation reaction allows for oxygen isotope exchange between the diffusing interstitial O_2 and the SiO_2 network.

In summary, the O_2 molecule may form ozonyl linkages in the oxide overcoming a barrier of $\sim$ 1.3 eV. This barrier is higher than the diffusion barrier in the dominant voids, but smaller than the diffusion barrier in small voids and the incorporation energy of free O_2 making reactions at the oxide interfaces more likely.

Diffusion of H_2O and O_2 in interstitial paths.

Representative results for the diffusion of H_2O through the ring structure of the SiO_2 network are shown in Fig. 13. Fig. 13a shows two 6 member Si-O rings. A water molecule diffuses across these rings along the shaded path. These rings constitute the bottlenecks of the diffusion channel. Fig. 13b depicts the total energy variation along the diffusion trajectory showing a 0.84 eV barrier in this particular channel. Since total energies – and consequently diffusion barriers – depend on the local bonding environment in an amorphous solid, we have calculated the barrier for both H_2O and O_2 diffusion in channels of different sizes. The results are summarized in Table 4, showing that the two molecules behave very differently.

Water molecules exhibit a barrier of 0.8-0.9 eV in all the six- and seven-member rings that increases abruptly to more than 2 eV for smaller rings. If we assume that there are continuous diffusion paths made up by six- and higher-member rings, the diffusion activation

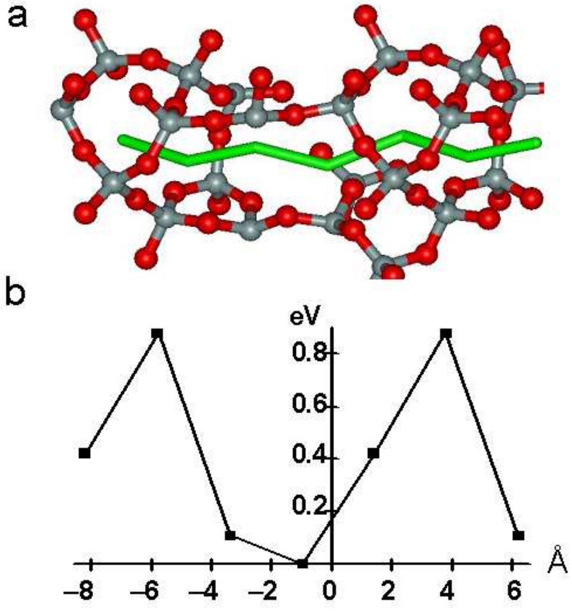

Figure 13: a) H_2O diffusing through two 6 member Si-O rings. b) Total energy variation along the above path. Black spheres are oxygen, gray spheres are silicon, and white spheres are hydrogen atoms.

energy would be 0.8-0.9 eV. Such an interpretation is fully consistent with the activation energies obtained in tritiated-water experiments[99] and thermal oxidation of Si[32]. Thus, the theoretical results confirm the interpretation of the experimental data in terms of diffusing water molecules. This mechanism is similar to that elucidated in previous calculations in quartz [100].

The results for O_2 molecules are very different. The diffusion barrier is extremely sensitive to the local topology and varies almost continuously from 0.6 to 1.5 eV for seven- and six-member rings with different topologies and continues to increase with five- and four-member rings. This wide variation is consistent with the experiments of Ref.[37] where activation energies in the range 0.7-1.5 eV were found in oxides grown in different ways. Deal and Grove[32] and others[101] extract an activation energy of $\sim$1.3 eV from oxidation data, but this energy includes the “incorporation energy” for oxygen molecules which was recently reported to be 0.4 eV [98]. These experiments suggest that there are diffusion paths along which the barrier does not exceed 0.9 eV. Our amorphous cells are not large enough to allow calculation of the statistical distribution of different types of six-member rings. Ultimately, only finite-temperature simulations in large cells can produce reliable theoretical predictions of the effective activation energy in different oxides. Such calculations are not currently practical.

Reaction of H_2O and O_2 molecules with oxygen vacancies

Oxygen vacancies are ubiquitous defects in all forms of SiO_2. They are electrically active as they may capture holes and consequently modify the I-V characteristics of MOS transistors. In optical fibers the neutral vacancy or the Si-Si bond gives rise to absorption and subsequent photoluminescence bands[39]. Under intense irradiation conditions, typically with doses exceeding several Mrads, oxygen vacancies may be created by dislodging network oxygens[87]. Neutral oxygen vacancies may capture holes since they have a partially occupied energy level in the band gap ~3.2 eV above the top of the valence band. This level is associated with dangling Si sp^3 orbitals.

Experiments show that the generation rate for E' centers (charged oxygen vacancies) is higher in "wet" synthetic silica (e.g., Suprasil-1) than in "dry" silica (e.g., Suprasil-W1)[87]. The "wet" oxide contains typically $10^{19} cm^{-3}$ OH groups (in form of silanol or interstitial water molecules), while the typical OH concentration in "dry" oxides is only $10^{16} cm^{-3}$. Also, infrared photoluminescence measurements show that, in the same type of dry oxides the concentration of interstitial O_2 molecules is $\sim 10^{18} cm^{-3}$, while in wet oxides it is $< 10^{14} cm^{-3}$[36]. Practically, these data mean that one has roughly 1000x more interstitial H_2O and 1000x less interstitial O_2 molecules in wet oxides than in dry ones. It is straightforward to assume that in bulk oxides radiation generates oxygen vacancies by the same mechanism regardless of the processing of the oxide (i.e., the cross section for dislodging oxygen atoms depends only on the local electronic environment surrounding the O atom and not on process-specific factors such as e.g., defect concentrations). In such case the difference in the generation rate of E' centers in various oxides is due to the different annihilation mechanisms of the E' centers.

We have investigated the reactions of charged and neutral oxygen vacancies with intersti-

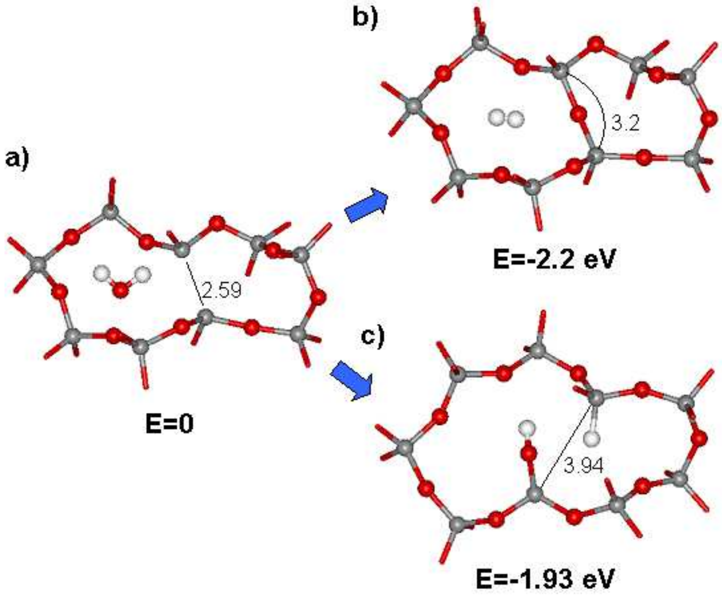

Figure 14: Reactions of H_2O with an oxygen vacancy (Si-Si bond). a) Initial position of a H_2O molecule in the middle of a 6-member ring with an O vacancy. b) Restored network with an interstitial H_2. c) Adjacent Si-OH and Si-H defects. Notice the relaxation of the ring by the different values of the Si-Si distance.

tial H_2O and O_2 molecules (Figs. 14,15). Annihilation of these defects is always exothermic, i.e., results in an energy gain above 1.4 eV. In case of O_2 molecules there is no barrier for the annihilation reactions, however for H_2O one or two O-H bonds must be broken to create the final reaction products, giving rise to a barrier.

Neutral oxygen vacancies usually relax to form strained Si-Si bonds as in Fig. 14a. A water molecule may fill up this vacancy and leave an interstitial H_2 behind (Fig. 14b) or create adjacent Si-OH and Si-H defects (Fig. 14c). To calculate the energy barrier of these reactions we move the oxygen atom of the H_2O molecule toward the centre of the Si-Si bond by varying the distance d_1 on Fig. 16a. The water molecule first has to disrupt the strained Si-Si bond that takes place at $d_1 \approx 1.2\AA$. At this location, the whole molecule binds to one of the Si atoms creating a metastable configuration. To proceed further, we now keep the O in the H_2O fixed and pull one of the hydrogens toward the other silicon by varying the distance d_2 (Fig. 16a). At $d_2 <\sim 2\AA$ the O-H bond breaks and the hydrogen binds to the adjacent Si. The total energy of the system is now lower, but it had to overcome a $\sim$1.8 eV barrier to reach the final configuration. We found that filling the vacancy with an O atom and leaving an interstitial H_2 would have a much higher barrier since two O-H bonds would need to be broken in addition to the weak Si-Si bond.

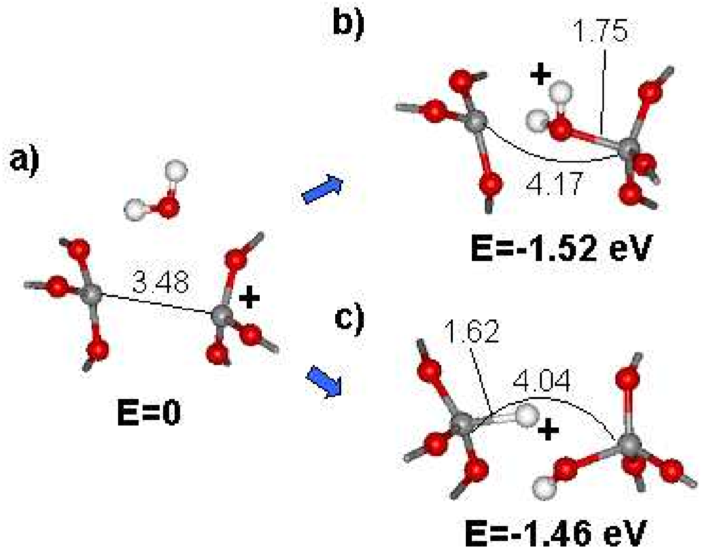

Figure 15: Reactions of H_2O with a positively charged oxygen vacancy (E'$_\delta$ center). a) Initial position of a H_2O molecule in the middle of a 6-member ring with an E'$_\delta$. b) H_2O bound to a positively charged Si atom. c) Adjacent Si-OH and Si-H^+ defects.

E' centers have several distinct equilibrium concentrations[21]. In the experimental study of Refs. [86, 87], the oxides were irradiated to several Mrads creating E' concentrations up to $10^{20} cm^{-3}$. The absence of subsequent thermal or electrical treatment results in the most abundant precursors (Si-Si bonds) to be transformed to E'$_\delta$ centers. These centers, which make up approximately 80% of the observed E' EPR signal, comprise two 3-fold coordinated Si atoms with a trapped positive charge (Fig. 15a)[21]. As opposed to the neutral case, these charged oxygen vacancies do not recombine forming an Si-Si bond. The Si-Si distance now is almost 3.5 $\mathring{A}$ as can be seen on Fig. 15. The interstitial H_2O is no longer in equilibrium; it immediately binds to one of the silicas as on Fig. 15b. To verify the absence of a barrier we have tracked the motion of the H_2O by fixing the distance between the O of the H_2O and the midpoint of the two silicon atoms (d_1 on Fig. 15b) and calculating the total energy of the relaxed supercell in each point. Looking at the energy levels in the band gap, we have determined that the positive charge is located on the H_2O molecule. The H_2O is in a metastable position on Fig. 15b, to arrive at the final configuration in Fig. 15c an O-H bond still has to be broken giving rise to a barrier.

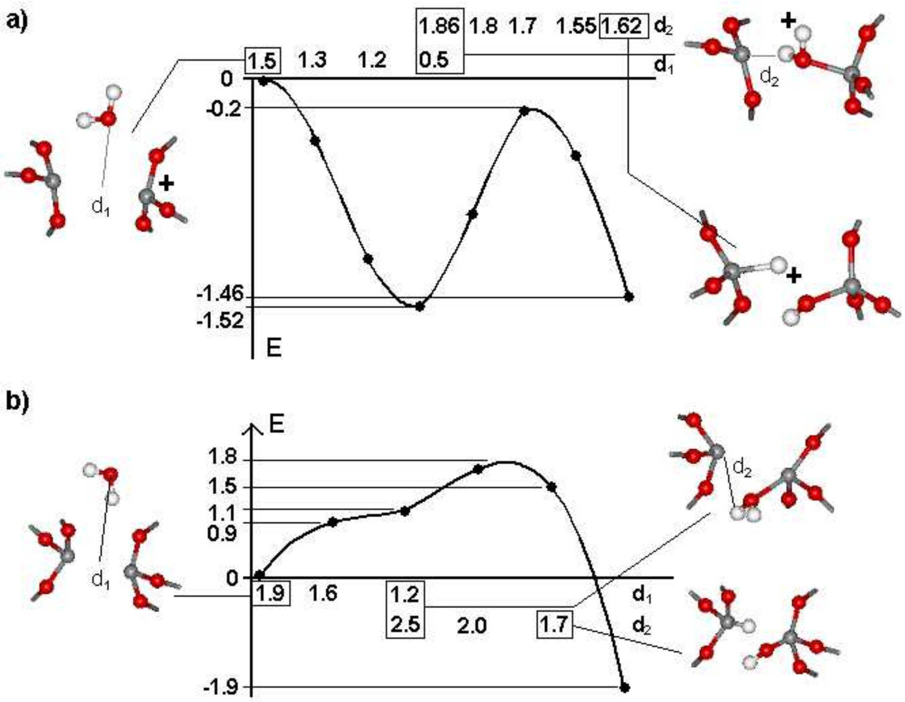

Figure 16: Energy barrier of the reactions annihilating neutral (a) and charged oxygen vacancies (b). a) At left is an H_2O molecule in a void with a vacancy as on Fig. 14. Total energies are obtained by first reducing d_1 then, at the flat part of the total energy curve, by keeping the O of the H_2O fixed and reducing d_2. At right are the final reaction products (bottom) and the intermediate stage with the H_2O bound to a Si (top). b) At left is a H_2O molecule in a void with an E'$_\delta$ center. First the H_2O binds to one of the silica in a barrierless reaction (right top). Then by keeping the O of the H_2O fixed an varying d_2 a Si-H^+ and a Si-OH is created (right bottom). The corresponding total energies at respective values of d_1 and d_2 are in the middle.

To calculate the barrier of this reaction, we have pulled one of the hydrogens of the water molecule toward the Si atom by varying the distance d_2 (Fig. 16b) and keeping the O of the H_2O fixed. At $d_2 <\approx 1.7\mathring{A}$ the Si-O bond breaks and the H attaches to the neighboring oxygen. The total energy of the system is almost the same as it was before the reaction, but it had to overcome a barrier of $\sim$ 1.3 eV. In this final configuration there are no dangling Si bonds, and an analysis of the defect states in the gap shows that the positive charge is located on the hydrogen of the Si-H complex.

We have found that O_2 molecules behave very differently in the vicinity of vacancies. For both neutral and charged vacancies, a peroxy linkage is formed in a barrierless reaction. The peroxy linkage has a doubly occupied state in the SiO_2 band gap about 0.8 eV above the top of the valence band. Therefore, we assume that the positive charge is localized on the oxygens building up the peroxy bond. Indeed, the geometrical configuration of the positively charged peroxy linkage is somewhat different from the neutral one on Fig. 11b with the Si-O distances increased to 1.75 and 1.97 $\AA$ and the O-O distance reduced to 1.37 $\AA$. The Si-Si distance was also larger, 4.31 $\AA$ instead of 3.79 $\AA$

Comparing the above data with diffusion barriers of O_2 and H_2O in the dominant voids of the oxide, we infer that in wet oxides the E'_δ center annihilation is reaction limited (by a 1.3 eV energy barrier) and charged vacancies are annihilated easier than neutral ones whereas in dry oxides the annihilation of E'_δ centers is diffusion limited with a lower activation barrier of ~ 1 eV that corresponds to the diffusion barrier of O_2 molecules. As a result, dry oxides will have a smaller concentration of E' centers than wet oxides when irradiated with the same total dose.

Conclusions

In summary, we have shown that, although the most stable form of water in SiO_2 is the interstitial molecule, vicinal silanol groups may form at a low energy cost (0.3 - 0.7 eV) with a barrier of 1.5 eV. H_3O^+ and OH^- complexes may form at an energy cost of 0.3 eV with a barrier of 1.5 eV in the large voids of the oxide and at high interstitial water concentrations, when clustering of H_2O molecules becomes significant. Water is more likely to split into OH^- and H^+ than neutral species if the oxide is irradiated, although this reaction –as all other reactions– has a barrier too high to be thermally activated.

O_2 molecules are most stable in the ozonyl linkage configuration; however, their formation is suppressed in the bulk oxide because of the high reaction barrier compared to the O_2 diffusion barrier. At the interfaces, however, ozonyl linkages may form because of the high incorporation energy of free O_2 molecules and the higher proportion of smaller rings, explaining the oxygen exchange patterns found in experiments.

Finally, we have shown that E' centers are annihilated at a faster rate in dry synthetic silica than in wet because the diffusion barrier of O_2 molecules that limits the annihilation process in dry oxides is lower than the rate limiting E'-H_2O reaction barrier in wet oxides.

CHAPTER V

ROLE OF ATOMIC AND ELECTRONIC RELAXATIONS IN THE OPTICAL SPECTRUM OF DEFECTS IN SiO_2

Investigation of the optical spectra of defects in oxides and semiconductors plays an important role in the study of defect structures, often complementing other techniques such as, e.g., electron paramagnetic resonance (EPR) spectroscopy. In particular, parameters extracted from optical absorption (OA) and photoluminescence (PL) spectra (e.g., location and width of optical bands, transition matrix elements or lifetimes of excited states) supply crucial information about the electronic structure of defects.

Stokes shifts exhibited by the optical spectra of molecules and of defects in solids are generally attributed to atomic relaxations in the molecule or in the atomic environment surrounding the defect in a solid. Using results of first-principles calculations on two distinctly different defects in SiO_2 we show that in solids, slow, non-radiative electronic relaxations may also contribute to the observed Stokes shift, complementing atomic relaxations. The two defects reported as examples (the non-bridging oxygen (NBO) atom and the interstitial OH molecule (OH_i)) have similar excitation spectra but different luminescence properties. The NBO atom has a very sharp luminescence line centered around 1.9 eV (620 nm), whereas OH_i molecules have a wide emission spectrum ranging from the infrared (0.8 eV or 1200 nm) to visible red (1.8 eV or 630 nm). Investigation of the results shows that the difference in the emission spectra is due to the different extent of atomic and electronic relaxations around the two defects; in the case of NBO site-independent electronic relaxations are responsible for the defect emitting a photon only at a particular energy, whereas in the case of OH_i molecules an interplay between site-dependent atomic and (therefore site-dependent) electronic relaxations result in a wide emission spectrum. A further, intriguing result is that both defects show similar vibrational and polarization properties; therefore, their contribution to the red luminescence band of irradiated amorphous SiO_2 may not have been decoupled in previous studies.

Introduction

The difference between optical absorption (OA) and ensuing photoluminescence (PL) energies –the Stokes shift[103]– is generally attributed to atomic relaxations of the defect or of the embedding medium. With the advent of quantum mechanics, the Franck-Condon (FC) principle offered an explanation for the effect by noting that electronic transitions and the accompanying electronic relaxations occur on a much faster time scale than atomic relaxations. Thus, the Stokes shifts exhibited by the optical spectra of defects in semiconductors and insulators are generally attributed to *slow lattice relaxations* that occur after optical excitation but prior to luminescence and are known as FC shifts[104].

The Koopmans approximation[105] offered a way to calculate transition energies as the difference in one-electron energy eigenvalues of the participating states. In the case of defects with localized energy levels in the gap, this transition energy is increased due to electron-electron repulsions (Hubbard U[106]) when a band electron is excited into a localized level that already contains an electron.

In this chapter we report results of first-principles calculations that reveal a novel behavior in certain defects in SiO_2. In particular, we focus on the optical properties of two defects that are unique in the sense that they have similar excitation and luminescence (PL) spectra despite the differences in their structure and chemical composition. The similarities and differences in their optical behavior are explained from the details of their atomic and electronic relaxation processes that take place between the optical excitation and luminescence.

We first study a defect that has an associated optical absorption (OA) band centered around 4.8 eV (with bandwidth ∼1 eV) and a subsequent sharp PL band centered at 1.9 eV (with bandwidth ∼0.18 eV). Direct optical excitation in the 1.9 eV band is also possible, though the efficiency of such a process is very low. The excitation energy in this case is centered around 2.0 eV. All three optical bands were invariably attributed to non-bridging oxygen (NBO) atoms, that is an oxygen atom bound to only one silicon with an unpaired electron in its non-bonding 2p orbital[107, 108]. The NBO was first observed in EPR measurements of irradiated, high OH-containing SiO_2 glass[109]. The EPR signal was found to correlate reasonably well with the 1.9 eV PL intensity, although it was suggested that other defects may also contribute to the luminescence[110]. Also, several cluster calculations argued that the electronic structure of the NBO allows for the observed PL line [111].

Based on results of first-principles calculations we show that the relatively large difference between the main OA and PL energies for the NBO defect is entirely due to slow, non-radiative electronic relaxations inside the SiO_2 valence band. During this electronic relaxation process, a deep valence hole, which has been created in the excitation process "bubbles up" to the valence band edge by a cascade of one-phonon electronic transitions which is unique to the solid state because it requires a continuum of higher-lying electronic states to be present. This electronic relaxation process –a form of "electronic" Franck-Condon (FC) shift– is suggested to have broad applicability in defining the optical behavior of defects in various media. Thus, the "electronic" FC shift would be a complementary process beside atomic relaxations that are usually attributed to determine the Stokes shift in defects.

In contrast to the NBO atom, with the help of calculations we have identified another defect –the interstitial hydroxyl molecule (OH_i)– which has a virtually identical excitation band. This defect may emit, however, at a range of PL energies including the well-known red PL band at 1.9 eV previously associated solely with NBO atoms. OH interstitials are difficult to observe directly because of their high reactivity and diffusivity. (The NBO center is also reactive, but localized.) However, as an iterim product, they may be created by the radiation induced dissociation of water molecules[89] or by water molecules reacting with NBO centers or peroxy radicals in the oxide[112]. Direct EPR observation of interstitial neutral OH groups was possible only in sodium-silicate glasses with water content above 2% by weight[112].

The broad emission spectrum of the OH_i defect is a result of the presence of both electronic and atomic relaxation processes with relaxation energies dependent on the local environment in the amorphous solid. The electronic relaxation process is the same as in the NBO defect, i.e., is related to a bubbling up of a deep valence hole to the top of the valence band via a cascade of one-phonon electronic transitions. In the atomic relaxation process, the excited OH_i moves closer to a network Si atom because of Coulomb attraction. Thus, the Stokes shift in this case results from a mix of electronic and atomic FC-shifts.

We found that the total energy gain in both electronic and atomic relaxation processes is sensitive to the Coulomb potential at the site where the hole is located. This potential is site-independent in case of the NBO defect; however, for OH_i-s it depends on the initial position of the OH molecule. Thus, the proximity of the OH_i molecule to the amorphous network determines the atomic relaxation energy and the extent of charge transfer to the interstitial OH molecule. The sum of the atomic and electronic relaxation energies turns out to be strongly site dependent, explaining a widening of the PL spectrum.

Relaxation processes and optical properties of non-bridging oxygen atoms

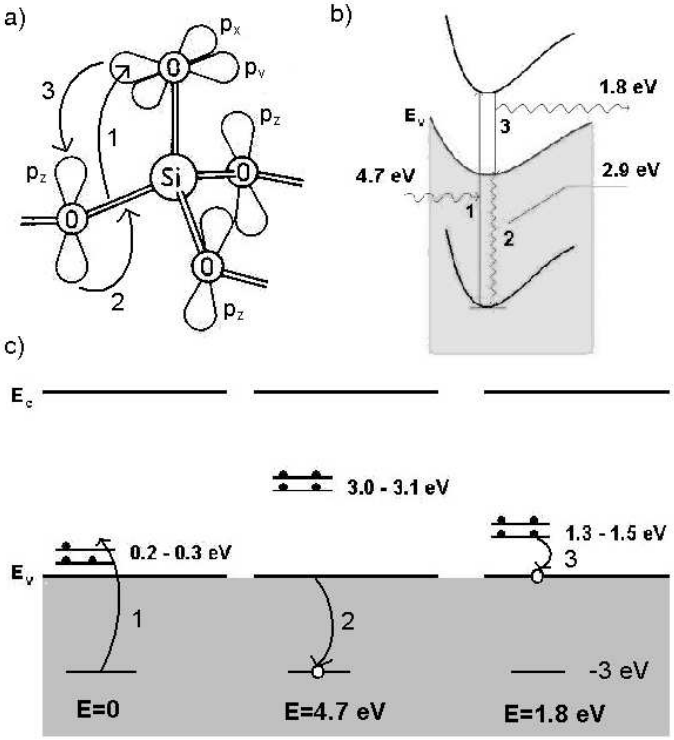

Figure 17: a) Schematics of the three main electronic processes responsible for the absorption and photoluminescence spectra of NBO. b) Total energy diagram as a function of a generalized coordinate. Absorption (1), luminescence (3) and *slow electronic relaxation* (2) processes are shown with their respective transition energies. c) One-electron energy level diagram of the NBO just before the corresponding transitions. The total energies of the system in these states (relative to the ground state) are shown in the bottom.

We find that, in its ground state, the NBO has two levels slightly above the valence band edge (E_v); one of them is filled by two electrons while the other one is populated by only one (Fig. 17c, left diagram). These are non-bonding 2p orbitals that naturally lie very close to E_v, which is made up of similar orbitals of the fully coordinated O atoms. The similar character of the defect states and the orbitals constituting the valence band edge suggests that optical excitations from the valence band edge are suppressed and more likely to originate from deeper valence levels. This observation is consistent with the fact that the OA spectrum is a broad band and is centered at an energy much higher than the position of the defect levels (4.8 eV) [39].

To find the possible initial states for optical excitation, we calculated the optical matrix elements for transitions from deep valence levels to the partially occupied level of the NBO. Our results show that these matrix elements are approximately constant when the initial state belongs to the upper half (0-6 eV region) of the valence band. To determine the orbital nature of the candidate initial states for the optical excitation, we calculated the valence-band density of states (DOS) and compared it to UV photoabsorption spectroscopy maesurements (Fig. 18). As can be seen, the 0-6 eV region of the valence band is composed mainly of a combination of Si sp^3 and a combination of the O $2p_x$ and $2p_y$ states where the orientation of the y axis is in the Si-O-Si plane perpendicular to the Si-Si line, i.e., the O $2p_y$ states are only weakly overlapping with Si sp^3 (see Fig. 18 and Ref. [4] for details).

Fig. 19 shows the optical absorption coefficient as a function of ($E = \hbar\omega$-0.3 eV) where $\hbar\omega$ is the photon energy, and 0.3 eV is the distance between the top of the valence band and lowest unoccupied non-bonding 2p orbital of the NBO defect. The calculations have been performed in the one-electron approach, i.e., we did not take into account the shift of the 2p levels due to the Coulomb repulsion. This shift would increase the energy required for excitation, therefore the $\hbar\omega$ photon energies do not correspond to the experimentally observed excitation energies. The absorption coefficient plotted as a function of ($\hbar\omega$-0.3 eV) shows how strongly the optical transition matrix element depends on the initial band number. We found that the matrix elements are approximately constant in the 0-6 eV region because the optical absorption curve nearly coincides with the density of states (DOS) curve. Therefore, the energy region near the DOS maximum (i.e., about 3 eV below E_v) gives the

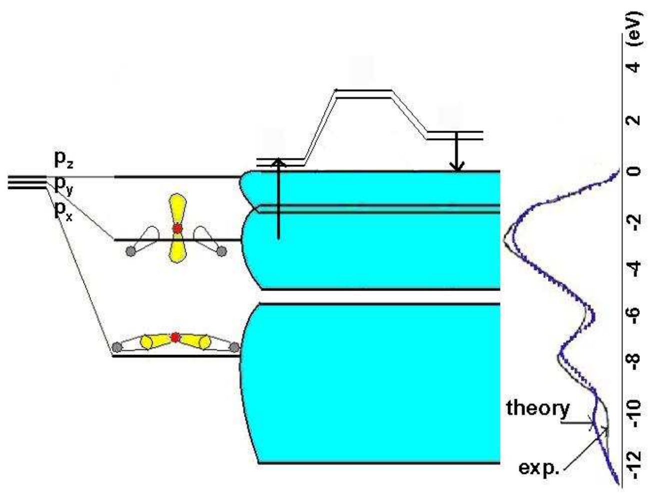

Figure 18: Left: band structure of SiO_2 with the energy levels of a NBO defect in the band gap. $2p_x$ lies along the Si-O line strongly overlapping with Si sp^3, $2p_y$ is in the Si-O-Si plane only weakly overlapping with Si sp^3. The non-bonding $2p_z$ orbitals (not drawn) are perpendicular to the figure. The arrows indicate the transitions to and from the NBO levels in the OA and PL processes. Right: density of states from UPS measurement[102] and our calculations

main contribution to the optical absorption spectrum when the final state is the NBO defect level (process 1 on Fig. 17a, c). Subtracting the total energy of the ground state NBO supercell from the energy of the supercell containing a valence hole at $\sim$ 3 eV below E_v and the excited defect we find 4.7 eV for the energy of excitation, in good agreement with the experimental 4.8 eV. The variation in excitation energy with respect to the position of the NBO atom within the supercell was within the accuracy of our calculations.

This excitation energy is apparently higher than what one would expect to obtain from the one-electron energy level positions of the participating states (i.e., $0.3 + 3.0$ eV < 4.8 eV). This difference is a result of many-body effects that are not taken into account in the calculation of the one-electron energy eigenvalues. However, some of these many-body effects are included when one calculates the optical transition energies as a difference between the total energies in the final and initial states.

After such an excitation occurs, we are left with a hole in the valence band (at $\sim$ 3 eV below E_v) and a negatively charged NBO atom. The NBO 2p levels experience a large Hubbard U shift; the one-electron energy spectrum calculated in the excited state shows that

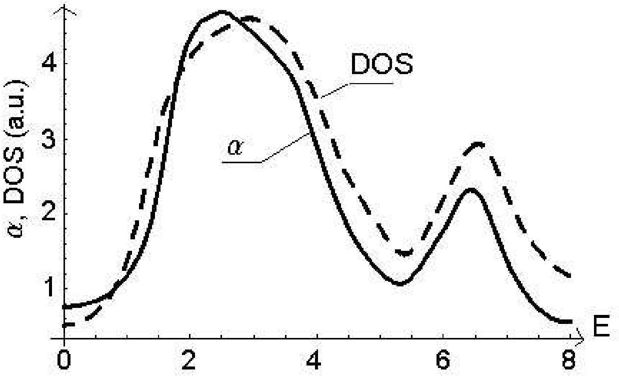

Figure 19: Absorption coefficient ($\alpha(\hbar\omega$-0.3 eV)) for the transitions into the lowest uoccupied level of the NBO defect compared with the DOS for the valence band (zero of energy for DOS corresponds to E_v, the energy axis is directed towards decrease of the energy). The units for both of the curves are arbitrary.

these levels shift up and are now located at $\sim$ 3 eV above E_v. In a subsequent process an electron has to deexcite from one of these defect orbitals or higher lying valence band states to the level of the deep valence hole. However, the calculated optical matrix elements for such transitions are small since both levels have substantial p-character. As a result, it is easier for the system to lower its energy by the deep valence hole "bubbling up" to the valence band edge in a phonon-assisted mechanism (process 2 on Figs. 17a, c). Although we did not investigate the participating phonon modes in detail, for the purpose at hand it is sufficient to note that the phonon-assisted bubbling up of the hole is a non-radiative process which is slow in comparison with the characteristic times typical for the electronic transitions. In the following we will refer to this process as to a "slow, non-radiative electronic relaxation," since it actually involves a charge redistribution within the valence band.

In order to study the charge distribution around the deep hole and the corresponding charge relaxation mechanism, we have plotted the difference between the charge densities of a supercell containing the deep hole state and a supercell containing the hole on the top of the valence band (Fig. 20). During the electronic relaxation process the charge is shifting from the dark shaded clouds into the light shaded areas. This effect is most pronounced around the oxygen atoms adjacent to the Si atom connected to the NBO and at the NBO itself. Apparently, the participating electronic states are delocalized (they are "smeared out" around at least 4 O atoms, although a similar, but smaller charge shift can be observed around *all* network O atoms). We also notice that the light shaded clouds that represent the charge around the deep hole (this is the charge that is "missing" from the supercell that includes the deep hole) are aligned in the Si-O-Si plane perpendicular to the Si-Si line. These clouds are the actual O 2p$_y$ states that – weakly interacting with Si sp^3 states – contribute in the formation of the upper part of the valence band. As a contrast, the dark shaded clouds are oriented perpendicular to the Si-O-Si plane. These are non-bonding O 2p$_z$ orbitals that make up the top valence band orbitals. This confirms our previous assumption that the electronic relaxation involves transitions mainly between oxygen p-like orbitals. The physical charge redistribution within the valence band alters the local electrostatic potential around the NBO atom. As a result of this, the defect energy levels are again shifted, albeit by a lesser extent than following the excitation process, since the total negative charge located at the NBO defect does not change.

During the initial excitation and subsequent electronic relaxation processes the system is nearly "frozen", i.e., no change in the atomic positions could be observed. The total energy difference between the initial and final stage of the electronic relaxation process is 2.9 eV which equals the Stokes shift associated with the studied OA/PL processes.

The last stage of the NBO associated OA/PL cycle is the deexcitation of an electron from the NBO defect level in the gap to the hole state located at the top of the valence band. Comparing total energy differences, a PL energy of 1.8 eV is obtained, which is again in excellent agreement with experiments[107, 108] (process 3 in Fig. 17a, c).

A reverse process, namely, the electronic excitation from the top of the valence band to the NBO defect level in the gap, also exists. Experimentally it was found that the absorption band corresponding to this process is observed at 2.0 eV[107, 108]. In this case no electronic relaxations are present, therefore the PL is exactly the reverse of the OA process and naturally has the same energy. Since the participating electronic states are almost purely O 2p states, this OA/PL cycle will have a lower intensity than the cycle where the initial excitation occurs at 4.8 eV.

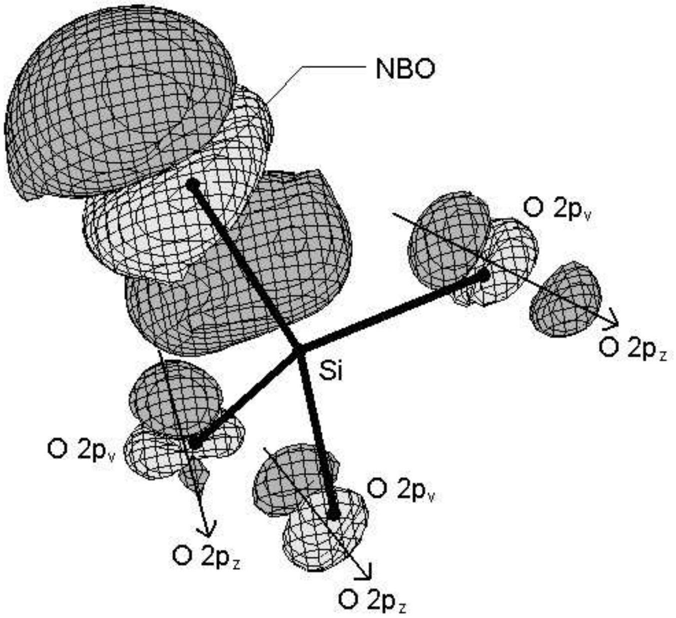

Figure 20: Difference of the charge densities of the supercell before and after electronic relaxation. The dark areas correspond to the areas that contain more charge before relaxation. During the relaxation process, this charge is transferring to the light colored areas. The dark areas can be identified as the O 2p$_z$ states that are filled before relaxation whereas the light areas mainly consist of the O 2p$_y$ states that contribute into the deep valence hole state and are therefore unoccupied. After the relaxation process the situation reverses: the O 2p$_z$ states (dark clouds) become unoccupied while the O 2p$_y$ states (light clouds) become occupied.

In this subsection we have shown that the NBO defect has a main absorption peak at 4.7 eV and an associated PL band at 1.8 eV. The relatively large Stokes shift is exclusively due to slow, nonradiative electronic relaxations inside the valence band.

Relaxation processes and optical properties of OH$_i$ molecules in a-SiO$_2$

Using the same calculational tools and approaches as in the case of the NBO, we have identified another defect – interstitial OH groups – which has a very similar optical signature. Since the 4.8 eV OA and the 1.9 eV PL is primarily observed in high-OH containing irradiated oxides, we suggest that this defect may also contribute to the optical processes in question.

Various configurations of OH groups in a-SiO_2

Neutral OH_i-s have two distinct equilibrium positions in a-SiO_2; they are either H-bonded to a network O atom or O-bonded to a network Si atom by a dipole interaction (shifts in the O-H vibrational frequency suggesting the existence of H-bonded OH were observed in infrared measurements[78]). This weak binding can be understood in the ionic picture of SiO_2; network O-s accumulate most of the negative charge and therefore they attract the positive (H) end of the OH dipole. Similarly, network Si atoms are somewhat positively charged; therefore, they attract the O atom of the OH dipole. In each case it costs ~ 0.3 eV to move the OH group in the middle of the void, where it is approximately equidistant from all nearest oxygens and silica. Because of the partial electronegativity of the O atom and the fact that it needs one electron to complete its second electron shell, the energy levels of the electrons in the OH^- configuration shift down with respect to the neutral configuration (Fig. 21). This indicates that the negatively charged state is more stable than the neutral for the interstitial OH group, therefore free OH groups are likely to act as electron traps. In the negative charge state, however, OH^- binds only to network Si atoms making them 5-fold coordinated.

The OH_i-related optical cycle

A neutral OH molecule has two levels in the band gap that are of oxygen 2p character just like the NBO (Fig. 22). Since the oxygen atom is bound to H, not to Si as in the case of the NBO defect, these p- levels do not need to be close to E_v. In order to find the most probable candidate states in the SiO_2 valence band where an excitation may originate from, we have again calculated the optical matrix elements for the transitions from deep valence bands to the OH_i partially occupied level. The result is similar as in the case of the NBO, namely that the matrix elements are approximately constant for initial states lying within the upper part (0-6 eV, with E_v=0) of the valence band. Therefore the dominant contribution into the excitation spectrum should be coming from the energies close to the DOS maximum, namely, from the region $\sim$2.5-3.5 eV below E_v (Fig. 24). Comparing total energy differences we find that the excitation energy of the initial OA process should occur in the 4.7-5.0 eV range depending on the initial position of the OH_i. This excitation is represented as process

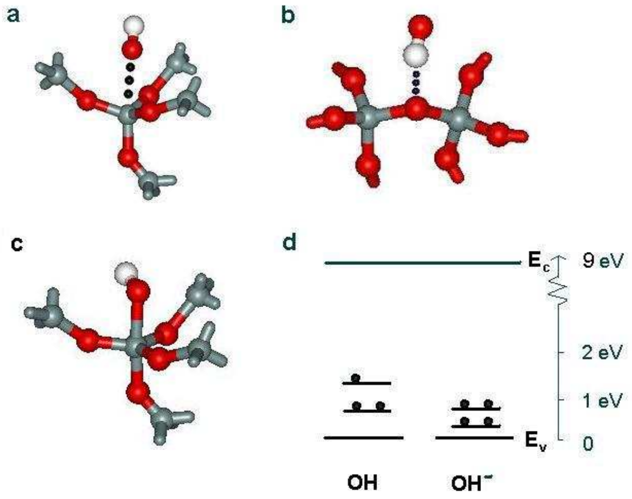

Figure 21: a) OH group weakly bonded to a network Si atom by a dipole interaction (represented by dots). b) OH group hydrogen-bonded to a network O atom. c) OH- group covalently bonded to a network Si atom making it 5-fold coordinated. d) energy levels of an OH group and an OH- ion in the band gap

1 in Fig. 22.

The excitation process produces a deep valence hole (as in the case of the NBO) and a negatively charged OH_i (OH^-). Analysis of the optical matrix elements for transitions from higher valence or defect levels to the deep hole state again suggests that optical deexcitation has very low probability. Similarly to the case of the NBO, the deep hole state prefers to "bubble up" to the top of the valence band in a slow, nonradiative phonon-assisted process (process 2 in Fig. 22). The electronic states participating in this relaxation process again have mainly O 2p-character as can be seen from a charge density difference plot (Fig. 25).

Despite the similarity in the physical nature of the excitation and electronic relaxation processes we find a very sensitive site-dependence for the energy release in the electronic relaxation process. To understand this phenomenon first we analyze the variation in excitation energies (Table 5), and compare the results with similar energies obtained for quartz (Table 5).

We found that the main reason for the decrease in excitation energies in smaller voids is that the OH_i is initially more "squeezed" to the network, therefore the overlap between the

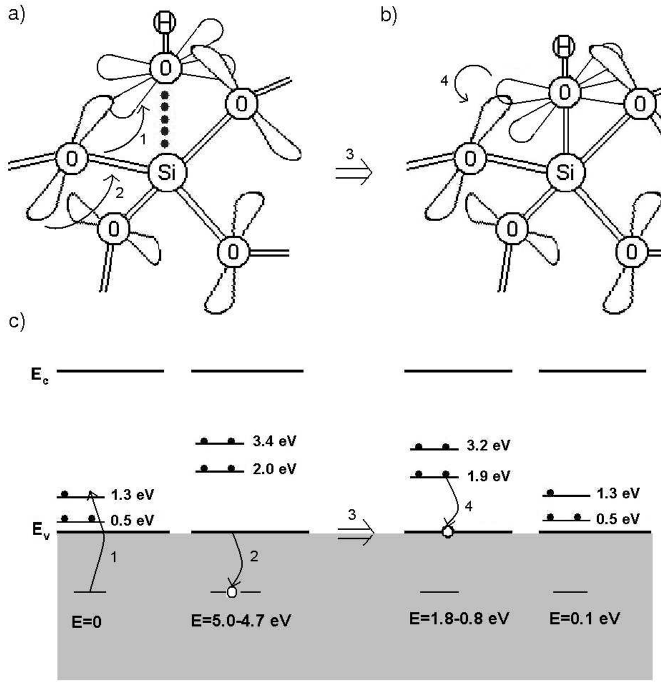

Figure 22: Schematics of the three main electronic processes (1,2 and 4) and the atomic relaxation process (3) responsible for the absorption and photoluminescence spectra of OH_i. a) Schematics and electronic transitions in OH_i. b) Schematics and the PL transition in (5)Si-OH^-. This defect forms as the charged OH_i relaxes and binds to a network Si. c) One-electron energy level diagram of the OH just before the corresponding transitions. The total energies of the system in these states (relative to the ground state) are shown in the bottom.

electronic wavefunctions of the states participating in the excitation process is greater than in the larger voids of the oxide. This leads to a lesser extent of charge separation between the network and the OH^-, i.e., the excited electron will have a part of its wavefunction still smeared around neighboring network atoms. The smaller charge shift leads to smaller Hubbard U effects that also reduce the total energy of the excited states. In larger voids, however, almost all of the excited electron will be located around the O atom of the OH^-, resulting in larger Hubbard U-s and excitation energies. To justify this assumption, we have calculated the increase in total charge caused by optical excitation inside a sphere having the cutoff radius ($R = 1.55\mathring{A}$) around the O atom of the OH molecule in voids of different sizes. As the data in Table 5 show the charge separation (i.e., the part of the electron localized

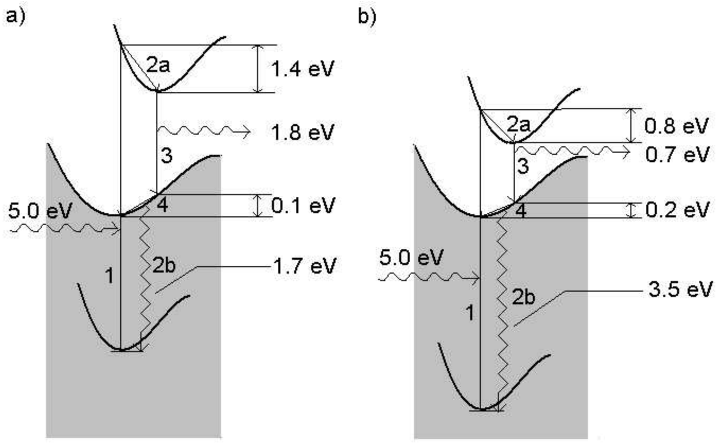

Figure 23: Total energy diagram as a function of a generalized coordinate illustrating the combined "atomic" and "electronic" FC-shift in a) a-SiO$_2$ with the OH in a large void, b) α-quartz.

over the OH$_i$) following the OA is smaller if the OH$_i$ resides in the smaller voids. In the case of quartz, the excitation energy is higher than in a-SiO$_2$, possibly because of differences in the band structure of the two materials. The small extent of charge separation, however, fits the tendency observed for a-SiO$_2$.

Table 5 shows that the electronic relaxation energy, which accounts for part of the Stokes shift, increases with decreasing void size. The site-sensitive nature of the relaxation energy is connected to the incomplete charge separation resulting from the excitation. Fig. 25 shows that, upon the electronic relaxation process, there is a significant change in the charge density distribution around the OH$^-$ molecule and adjacent network O atoms. In the case of the OH$^-$ a part of the binding O 2p$_x$ electron is being transfered to non-bonding O 2p$_y$ and 2p$_z$ orbitals. For network O atoms we observe a similar effect as in the case of the NBO – the charge transfers from O 2p$_y$ to non-bonding O 2p$_z$ orbitals. Again, this charge redistribution is more pronounced in smaller voids. The larger extent of the charge shift results in larger energy gains once the electron is transferred from one state to the other.

In the case of the OH$_i$ defect, there are also significant atomic relaxations (process 3 on Fig. 22) following excitation. This atomic relaxation is a result of a Coulomb electrostatic attraction between the OH group (negatively charged when an additional electron arrives

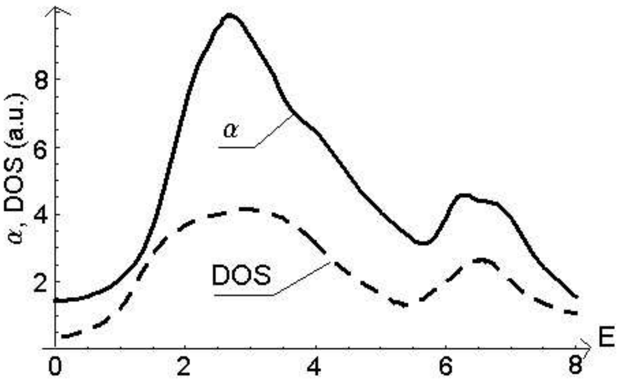

Figure 24: Absorption coefficient ($\alpha(\hbar\omega$-1.3 eV), where 1.3 eV is the energy of the lowest unoccupied OH_i defect level) for the transitions into the lowest unoccupied level of the OH defect compared with the DOS for the valence band (zero of energy for DOS corresponds to E_v, the energy axis is directed towards decrease of the energy). The DOS is scaled by the same factor as in the case of the NBO defect to see that $\alpha(OH_i) \approx 2 * \alpha(NBO)$.

to it as a result of excitation) and the Si atom. In this process the distance between the Si and the O atom from the OH group significantly decreases. Naturally, this process gives the largest energy gains in large voids (cf. Table 5). The reason for this effect is that both the charge separation and the displacement is larger in large voids resulting in a higher energy gain from the Coulomb interaction of the OH^- and the network accomodating the deep valence hole.

At the final stage of the atomic relaxation, the OH^- is at $\sim 1.8 \pm 0.1 \mathring{A}$ apart from the Si atom which is $\sim$ 10% longer than the average network Si-O bond. As can be seen on a 2-dimensional section of the charge density defined by the Si-O-H plane, Fig. 26, the excess electron binds the OH^- to network O atoms. Investigation of the partial density of states within a sphere of the Wigner-Seitz radius around the Si, adjacent O and H atoms reveals that the binding electron is located at the Si atom and at its 5 adjacent O atoms.

After the atomic and electronic relaxation processes we have a negatively charged OH group bound to a network Si atom and a hole at the top of the valence band. The following step is the deexcitation of the excess electron from the non-bonding OH 2p level to the valence band edge, resulting in the emission of a photon. This luminescence process is site-dependent, with energies distributed in the range 0.8-1.8 eV (process 4 in Fig. 22 and Table

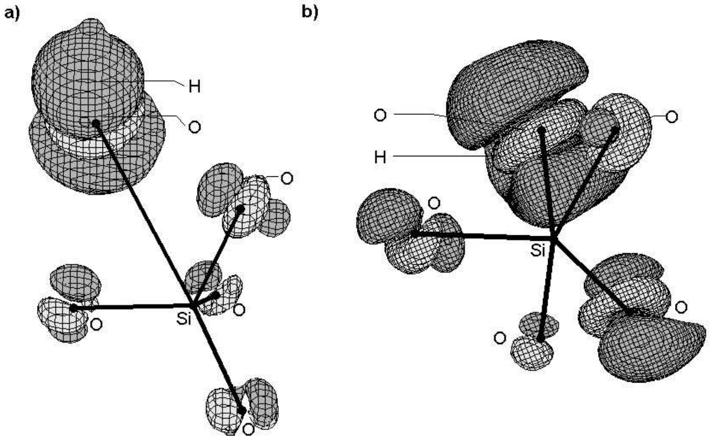

Figure 25: Charge density difference of the supercells before and after electronic relaxation at the OH_i. As in the case of the NBO, the dark areas contain more charge before relaxation, this charge is transferring to the light colored areas during the relaxation process. The dark areas are mainly the O $2p_z$ states that are filled before relaxation whereas the light areas are the O $2p_y$ states that contribute to the deep valence hole state and are therefore unoccupied. After the relaxation process the situation reverses: the O $2p_z$ states (dark clouds) will be unoccupied and the O $2p_y$ (light clouds) will be occupied. a) Results for OH_i in a ~ 6 $\mathring{A}$ void. b) Results for OH_i in a ~ 3.5 $\mathring{A}$ void. The extent of charge transfer during electronic relaxation is larger in smaller voids.

5).

This PL process restores the state of the supercell to its ground state configuration, however, at the initial moment after the PL, the neutral OH molecule is closer to the network than its equilibrium position. Thus, a final atomic relaxation process (not shown in the Figure 22) takes place resulting in a further, but very small energy release (typically ~ 0.1 eV in all cases) since the interaction between the neutral OH_i and the amorphous network is weak.

It is interesting to note that the numerical values of the square of the absolute value of the optical matrix elements for transitions from the deep valence band levels to the OH_i level are about twice the matrix elements for transitions to the NBO level (the "arbitrary units" for the absorption curves in Figs. 19, 24 are the same). Therefore once the total absorption coefficient is known, one can establish a relationship between the concentrations of the two defects.

Table 5: Variations in Si-O distance (in $\AA$), OA, relaxation and PL energies (eV) and charge transfer (e) in voids of different diameters ($\AA$).

void diameter	~6.0	~5.0	~3.5	~3.5 (α-quartz)
Si-O dist. before/after relaxation	2.34 / 1.87	2.20 / 1.77	2.07 / 1.71	1.87 / 1.69
OA energy	4.9	4.9	4.8	5.0
electronic/ atomic relaxation energy	1.7 / 1.4	2.1 / 1.4	3.1 / 0.9	3.5 / 0.8
total relaxation energy	3.1	3.5	4.0	4.3
PL energy	1.8	1.4	0.8	0.7
charge transfer	0.59	0.56	0.46	0.45

Excitation in the luminescence band may also exist by a similar mechanism as in the case of the NBO, i.e., an electron from the top of the valence band is excited to the partially occupied O 2p orbital in the OH molecule. Electronic relaxations are absent in this case, however the OH_i would still relax toward a network Si atom. The presence of atomic relaxations result in a non-zero Stokes shift, unlike in the case of the NBO. The Stokes shift decreases with void size as the atomic relaxations are smaller in smaller voids.

In summary, we have shown that OH_i-s have a main OA peak around 4.7-5.0 eV and a subsequent PL band at 0.8-1.8 eV depending on the initial position of the OH_i molecule. The sum of site-dependent electronic and atomic relaxations accounts for the observed Stokes shift, with atomic relaxation energies decreasing and electronic relaxation energies increasing in smaller voids.

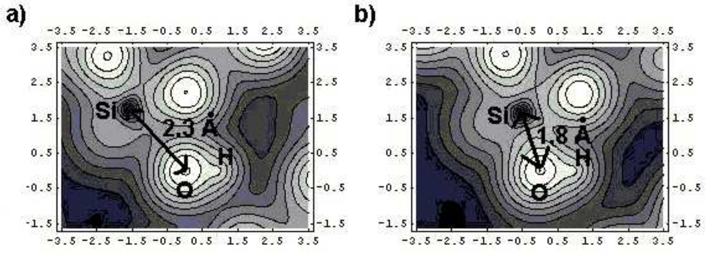

Figure 26: Charge density contours in the Si-O-H plane: (a) before, and (b) after atomic relaxation of the OH_i defect. The excess electron becomes delocalized over the O of the OH_i and several neighboring network atoms.

Relaxation processes and optical properties of OH_i molecules in α-quartz

Hydroxyl groups incorporate into the α-quartz crystal lattice during the synthetisation process where the ground silicate is usually dissolved in NaOH or $Ca(OH)_2$. They usually attach to group III impurities (e.g., to Al) that may substitute Si atoms[93]. Radiation may temporarily create interstitial OH groups by breaking up these bonds.

To study the site-dependent nature of the atomic and electronic relaxation processes, we have performed the same set of calculations in α-quartz as in the preceeding subsection. Here we only give a summary of the results.

Since α-quartz has a more rigid structure with predominantly smaller voids, we anticipate that the effects observed in the smaller voids of a-SiO_2 will be magnified. We find that the dominant excitations have an energy of 5.0 eV. The subsequent electronic relaxation is indeed relatively large (3.5 eV), whereas the energy gain from atomic relaxation is small, since the OH_i moves by only about $0.18\mathring{A}$ toward the Si atom. The PL energy is at the lower edge of the energy range observed for a-SiO_2 (0.7 eV); see Table 5. This result would suggest a possible way to verify the OH^-- related OA/PL cycle experimentally. This line however, has not been observed so far, possibly because of the low concentration of OH_i-s in α-quartz.

Experiments related to the 1.9 eV photoluminescence band in a-SiO_2

In this section we give a summary of the experiments that have been used to support the identification of the defect responsible for the 4.8 eV OA and 1.9 eV PL bands as NBO. We show that all of these observations are consistent with the OH_i-related OA/PL cycle as well.

A characteristic phonon sideband of the zero-phonon line (ZPL) of the 1.9 eV PL band has been observed at 0.11 eV (890 cm^{-1}) beside the main luminescence peak[107, 108]. This ZPL was suggested to be due to Si-NBO stretching vibrations since its frequency is close to the Si-O vibrational frequency in a silanol (Si-OH) complex (969 cm^{-1}) that was observed in Raman spectroscopy[113]. Our calculations give 860 cm^{-1} and 832 cm^{-1} for the vibrational frequencies of the NBO and Si-OH defects, respectively. The vibrational frequency for silanol has to be smaller than that of the NBO if the O and H oscillate in the same phase, because the mass of the oscillating particle (OH group vs. O atom) is larger. In the Raman-measurement, however, probably a mode is excited where the O and H atoms of the Si-OH complex oscillate out of phase.

For the calculated Si-O vibrational frequency in the (5)Si-OH^- complex we found 845 cm^{-1} in a-SiO_2 in the largest void and 910 cm^{-1} in α-quartz. Since the (5)Si-OH^- behaves in α-quartz similar to smaller voids in the amorphous oxide, we conclude that the ZPL of the OH^-related PL falls in the 840-910 cm^{-1} region, overlapping with what has been obtained for NBO. This result suggests that the OA/PL cycle originating from both defects is consistent with the ZPL measurement. The site-dependent vibrational energy of the (5)Si-OH^- complex gives a contribution to the phonon background of the time-resolved PL spectrum in the ZPL measurement. Shifts in this background should be observable in deuterated oxides since the (5)Si-OD^- defect would have a smaller vibrational frequency.

Upon excitation in the 4.8 eV OA band by linearly polarized light, the polarization degree of luminescence was found to be $P = -1.5\%$[107]. The polarization degree is defined via Eq. 41 involving the intensities of the photoluminescent light parallel (I_p) and perpendicular (I_p) to the incident beam. The polarization degree is also connected to the angle α subtended by the transition dipoles in the OA and the PL process according to [115]

$$P(\alpha) = \frac{I_p - I_h}{I_p + I_h} = \frac{3 \cdot \cos^2 \alpha - 1}{\cos^2 \alpha + 3} \tag{41}$$

The transition dipole is the integral of the dipole moment operator $e\mathbf{r}$ and can be calculated once the optical matrix elements –and thus the matrix elements of the momentum operator

$(-i\nabla)$– are known:

$$\mathbf{r}_{ab} = \langle\Psi_a|\mathbf{r}|\Psi_b\rangle = \frac{\hbar}{im_e}(E_a - E_b)\langle\Psi_a| - i\nabla|\Psi_b\rangle \tag{42}$$

where transitions occur from state Ψ_b with energy E_b to state Ψ_a with energy E_a.

Let us denote the ground state of the system by $|\Psi_a\rangle$, the excited state with the deep hole by $|\Psi_b\rangle$ and the excited state with the hole at the top of the valence band by $|\Psi_c\rangle$. Then the angle subtended by the absorption and luminescence dipoles is given as

$$\alpha = \arccos\frac{\mathbf{r}_{ab}\cdot\mathbf{r}_{ca}}{|\mathbf{r}_{ab}|\cdot|\mathbf{r}_{ca}|} \tag{43}$$

For the angle between the OA and PL dipoles we have obtained $\alpha = 62^o$ for NBO and $\alpha = 57^o$ for (5)Si-OH$^-$ in the large voids of a-SiO$_2$, $\alpha = 92^o$ for (5)Si-OH$^-$ in α-quartz. The experimentally observed value for the polarization degree corresponds to an angle $\alpha = 55.7^o$. The results correctly suggest that both the NBO and the (5)Si-OH$^-$ in a-SiO$_2$ has a low degree of polarization when excited in the 4.8 eV band. The higher polarization degree in α-quartz is probably caused by the different electronic band structure of the crystal lattice. Again, the differences between the results for NBO and (5)Si-OH$^-$ are too small to be able to distinguish between the two defects.

If the defect producing the 1.9 eV PL is excited in the 2.0 eV absorption band, the observed polarization degree is $P \approx 50\%$[107] implying an angle of $\alpha = 0$ or 180^o between the absorption and emission dipoles. This absorption corresponds to excitations from the valence band edge, i.e., no deep hole is created, therefore electronic relaxations are absent. For both defects, the electron is excited from non-bonding O 2p$_z$ orbitals constituting the top of the valence bands to the partially occupied O 2p orbital of the NBO or the OH$_i$, and the luminescence process is exactly the reverse of excitation. In case of the NBO defect no atomic relaxations are present either, so the absorption and emission dipoles would be exactly parallel. This is not true for OH$_i$-s because of the presence of atomic relaxations. The motion of the OH$_i$ toward the Si atom before PL will result in a small angle between the absorption and emission dipoles. Time-resolved PL emission polarization spectra upon excitation in the 2.0 eV OA band show that the polarization degree decreases (i.e., the angle

α between the OA and PL dipoles increases) at lower PL energies[108]. We suggest that the increase in α with decreasing PL energy occurs because, if the atomic relaxations are larger (i.e., if the OH_i moves a longer distance before PL and also takes away a larger part of the excitation energy), the OA and PL dipoles will subtend a larger angle.

The 1.9 eV PL is typically observed at low temperatures (below 110K)[108]. The reason for this is that both the NBO and the OH_i are radicals that can easily be passivated by other freely diffusing defects (e.g., hydrogen). Moreover, the OH_i can itself diffuse which, in addition to its high reactivity, is the reason why it was not observed directly in oxides with a conventional water content. Assuming that the OH_i is primarily created from interstitial water molecules that mostly reside in the large voids of the oxide, we have calculated the diffusion barrier for an OH_i through a channel connecting two large voids. The obtained 0.3 eV is in excess of the 0.3 eV "binding" energy that arises from a weak dipole interaction between the OH_i and network Si or O atoms (see Section). Therefore, via thermal excitations, the OH_i may become "free" i.e., its weak bond to the network can be disrupted and thereafter it cannot participate in the described optical processes. The energy necessary for breaking the weak bond between the OH_i and the network (0.3 eV) is comparable to the diffusion barrier for interstitial hydrogen (0.2 eV) [90]. This result shows that both the NBO and the OH_i defects are likely to disappear at the same temperature leading to the vanishing of the PL signature.

Finally, we point out that the red PL from the SiO_2 surface comes entirely from NBO defects because (5)Si-OH^- cannot form at the surface[116]. Since all surface Si atoms are undercoordinated, the addition of an OH^- group would not make a silicon atom 5-fold coordinated.

Conclusions

In summary, we have shown that electronic and atomic relaxations are complementary factors in determining Stokes-shifts at optically active defects in SiO_2. First we have carefully analysed the NBO defect that has been associated with a 4.8 eV and 2.0 eV OA and 1.9 eV PL band in a-SiO_2 and have shown that the large Stokes-shift is entirely due to slow, non-radiative electronic relaxations, in which a deep valence hole, created in the absorption process, “bubbles up” to the valence-band edge by a phonon-assisted mechanism. Using first-principles calculations, we have identified another defect –interstitial OH groups– that have a similar optical signature. For this defect, however, electronic and atomic relaxations are both responsible for the calculated Stokes-shift. The presence of atomic relaxations also introduces site-dependence in the observed optical spectra of the amorphous oxide. Experiments related to the 1.9 eV PL are consistent with both the NBO and OH_i defects.

BIBLIOGRAPHY

[1] R. L. Mozzi and B. E. Warren, J. Appl. Crystallogr. **2**, 164 (1969)

[2] J. R. G. DaSilva, D. G. Pinatti, C. E. Anderson and M. L. Rudee, Phil. Mag. **31**, 713 (1975)

[3] F. R. Boyd and J. L. England, J. Geophys. Res. **65**, 149 (1960)

[4] S. T. Pantelides and W. A. Harrison, Phys. Rev. B **13**, 2667 (1976)

[5] P. Balta and E. Balta, *Introduction to the Physical Chemistry of the Vitreous State* (Tunbridge Wells: Abacus) (1976)

[6] R. N. Nucho and A. Madhukar, Phys. Rev. B **21**, 1576 (1980)

[7] W. H. Zachariasen, J. Am. Chem Soc. **54**, 3841 (1932)

[8] J. T. Randall, H. P. Rooksby and B. S. Cooper B S, 2. Kristallographie **75**, 196 (1930)

[9] A. C. Wright and R. N. Sinclair, *The Physics of* SiO_2*, and its Interfaces* ed. S T Pantelides (New York: Pergamon) pp 133- (1978)

[10] J. H. Konnert and D. E. Appleman, Acta Crystallogr. B **34**, 391 (1978)

[11] W. G. Wyckoff, *Crystal Structures* vol I. (New York: Interscience) pp 312 (1963)

[12] see data on http://www.webmineral.com/data/tridymite.shtml

[13] S. T. Pantelides, Phys. Rev. Lett., **57**, 2979 (1986)

[14] J. M. Gibson and D. W. Dong, J. Electrochem. Soc. **127**, 2722 (1980)

[15] M. Hasegawa et al., Nucl. Instr. and Methods B **166-167**, 431 (2000)

[16] E. A. Taft, J . Electrochem. Soc. **125**, 968 (1978)

[17] W. L. Warren, E. H. Poindexter, M. Offenberg and W. Müller-Warmuth J. Electrochem. Soc. **139**, 872 (1992)

[18] R. A. Weeks, J. Appl. Phys. **21**, 1376 (1956)

[19] D. L. Griscom and E. J. Friebele, Phys. Rev. B **34**, 7524 (1986)

[20] K. C. Snyder and W. B. Fowler, Phys. Rev. B **48**, 13238 (1993)

[21] Z-Y Lu et al., Phys. Rev. Lett. **89**, 285505 (2002)

[22] R. A. B. Devine and J. Arndt, Phys. Rev. B **39**, 5312 (1989)

[23] R. A. B. Devine and J. Arndt, Phys. Rev. B **35**, 9376 (1987)

[24] M. E. Zvanut et al. Appl. Phys. Lett. **54**. 2118 (1989)

[25] D. L. Griscom, Nucl. Instruments and Methods, **B1**, 481 (1984)

[26] T. E. Tsai, D. L. Griscom and E. J. Friebele, J. Non-Cryst. Solids **91**, 170 (1987)

[27] V. A. Gritsenko, A. Shaposhnikov, G. M. Zhidomirov and M. Roger, Solid State Comm. **121**, 301 (2002)

[28] P. E. Bunson et al., IEEE Trans. Nucl. Sci. **47**, 2289 (2000)

[29] K. Klier and A. C. Zettlemoyer J. Colloid Interface Sci. **58**, 216 (1977)

[30] A. I. Moulson and J. P. Roberts, Trans. Brit. Cerm, Soc. **59**, 1208 (1960)

[31] P. J. Burkhardt, J. Electrochem. Soc. **114**, 196 (1967)

[32] B. E. Deal and A. S. Grove, J. Appl. Phys. **36**, 3770 (1965).

[33] E. H. Poindexter, J . Vac. Sci. Technol. A **6**, 1352 (1988)

[34] H. Wakabatashi and M. Tomozawa, J. Am. Ceram. Soc. **72**, 1850 (1989)

[35] R. H. Doremus, J. Mater. Res. **10**, 2379 (1995)

[36] L. Skuja, B. Güttler, D. Schiel and A. R. Silin, Phys. Rev. B **58**, 14296 (1998).

[37] J. J. Perez-Bueno, R. Ramirez-Bon, Y. V. Vorobiev et al., Thin Solid Film **379**, 57 (2000).

[38] D. L. Griscom, J. Non-Cryst. Solids **31**, 241 (1978)

[39] L. Skuja, J. Non-Cryst. Solids **239**, 16 (1998)

[40] P. Hohenberg and W. Kohn, Phys. Rev. **136**, B864 (1964)

[41] W. Kohn and L. J. Sham, Phys. Rev. **140**, A1133 (1965)

[42] J. P. Perdew, in *Electronic Structure of Solids '91* edited by P. Ziesche and H. Eschrig (Akademie-Verlag, Berlin, 1991)

[43] C. Filippi, D. J. Singh, and C. J. Umrigar, Phys. Rev. B **50**, 14947 (1994)

[44] A. Dal Corso, A. Pasquarello, A. Baldereschi, and R. Car, Phys. Rev. B **53**, 1180 (1996)

[45] G. Ortiz, Phys. Rev. B **45**, 11328 (1992)

[46] A. Khein, D. J. Singh, and C. J. Umrigar, Phys. Rev. B **51**, 4105 (1995)

[47] C. S. Wang, B. M. Klein, and H. Krakauer, Phys. Rev. Lett. **54**, 1852 (1985)

[48] P. Bagno, O. Jepsen, and O. Gunnarsson, Phys. Rev. B **40**, 1997 (1989)

[49] D. R. Hamann, Phys. Rev. Lett. **76**, 660 (1996)

[50] D. R. Hamann, Phys. Rev. Lett. **81**, 3447 (1998).

[51] G. D. Bachelet, D. R. Hamann, and M. Schluter, Phys. Rev. B **26**, 4199 (1982)

[52] P. E. Bunson, M. Di Ventra, S. T. Pantelides, R. D. Schrimpf and K. F. Galloway, IEEE Trans. Nucl. Sci. **46**, 1568 (1999)

[53] J. C. Philips and L. Kleinman, Phys. Rev. B **116**, 287 (1959)

[54] B. J. Austin, V. Heine, and L. J. Sham, Phys. Rev. **127**, A276 (1962)

[55] Y.-M. Juan, E. Kaxiras, and R. G. Gordon, Phys. Rev. B **51**, 9521 (1995)

[56] M. Fuchs, M. Bockstedte, E. Pehlke, and M. Scheffler, Phys. Rev. B **57**, 2134 (1998)

[57] A. Zunger and M. L. Cohen, Phys. Rev. Lett. **41**, 43 (1978)

[58] D. R. Hamann, M. Schluter, and C. Chiang, Phys. Rev. Lett. **43**, 1494 (1979)

[59] G. P. Kerker, J. Phys. C **13**, L189 (1980)

[60] D. Vanderbilt, Phys. Rev. B **32**, 8412 (1985)

[61] A. M. Rappe, K. M. Rabe, E. Kaxiras, and J. D. Joannopoulos, Phys. Rev. B **41**, 1227 (1990)

[62] N. Troullier and J. L. Martins, Phys. Rev. B **43**, 1993 (1991)

[63] D. Vanderbilt, Phys. Rev. B **32**, 8412 (1990)

[64] D. Vanderbilt, Phys. Rev. B **41**, 7892 (1990)

[65] P. E. Blöchl, Phys. Rev. B **41**, 5414 (1990)

[66] P. E. Blöchl, Phys. Rev. B **50**, 17953 (1994)

[67] D. J. Chadi and M. L. Cohen, Phys. Rev. B **8**, 5747 (1973).

[68] M. Ramamoorthy and S.T. Pantelides, Phys. Rev. Lett. **76**, 267 (1996) and Solid State Comm. **106**, 243 (1998)

[69] Y. Tu, J. Tersoff, G. Grinstein, and D. Vanderbilt, Phys. Rev. Lett. **81**, 4899 (1998).

[70] F. Wooten, K. Winer, and D. Weaire, Phys. Rev. Lett. **54**, 1392 (1985).

[71] M. C. Payne, M. P. Teter, D. C. Allan, T. A. Arias, J. D. Joannopoulos, Rev. Mod. Phys. **64**, 1045 (1992)

[72] H. Hellmann *Einführung in die Quantumchemie* Deuticke, Leipzig, (1937)

[73] R. P. Feynman, Phys. Rev. **56**, 340 (1939)

[74] G. Kresse and J. Furthmüller, Phys. Rev. B **54**, 11169 (1996).

[75] G. Hetherington and K. H. Jack, Phys. Chem. Glasses **3**, 129 (1962)

[76] R. Bruückner, Glastechnische Berichte **37**, 459 (1964)

[77] K. M. Davis and M. Tomozawa, J. Non-Cryst. Solids **185**, 203 (1995)

[78] K.M. Davis and M. Tomozawa, J. Non-Cryst. Solids **201**, 177 (1996).

[79] B. A. Proctor, I. Whitney and J. W. Johnson, Proc. R. Soc. **A297**, 534 (1966)

[80] J. C. Mikkelsen, Appl. Phys. Lett. **39**, 903 (1981).

[81] E. P. Gusev, H. C. Lu, T. Gustaffson and E. Garfunkel, Phys. Rev. B **52**, 1759 (1995).

[82] H. C. Lu, T. Gustaffson, E. P. Gusev and E. Garfunkel, Appl. Phys. Lett. **67**, 1742 (1995).

[83] J. R. Chelikowsky, D. J. Chadi and N. Binggeli, Phys. Rev. B **62**, R2251 (2000).

[84] L. Skuja, M. Hirano, H. Hosono, Phys. Rev. Lett. **84**, 302 (2000).

[85] R. H. Stolen and G. E. Walrafen J. Chem. Phys. **64**, 2623 (1976)

[86] R.A.B. Devine, Nucl. Instr. and Methods **B46**, 244 (1990).

[87] R.A.B. Devine, J. Non-Cryst. Solids **107**, 41 (1988).

[88] A. Bongiorno and A. Pasquarello, Solid-State Electr. **46**, 1873 (2002).

[89] Hwang et al., J. Chem. Phys. **110**, 4123 (1999)

[90] B. Tuttle, Phys. Rev B **61**, 4417 (2000)

[91] M. A. Szymanski, A. M. Stoneham and A. L. Schluger, Microelectr. Rel. **40**, 567 (2000)

[92] F. B. McLean, IEEE Trans. Nucl. Sci. **NS-27**, 1651 (1980).

[93] B. Subramaniam, L. E. Halliburton and J. J. Martin, Phys. Chem. Solids **45**, 575 (1984).

[94] A. Hartstein and D. R. Young, Appl. Phys. Lett. **38**, 631 (1981)

[95] E. H. Poindexter, Rep. Prog. Phys. **57**, 791 (1994)

[96] T. Bakos, S. N. Rashkeev and S. T. Pantelides, Phys. Rev. Lett. **88**, 055508 (2002).

[97] A. G. Revesz et al., Appl. Surf. Sci. **194**, 101 (2002)

[98] A. M. Stoneham, M. A. Szymanski, A. L. Schluger, Phys. Rev. B **63**, 241304(R) (2001)

[99] I. Burn and J. P. Roberts, Phys. Chem. Glasses **11**, 106 (1970).

[100] J. P. Hagon, A. M. Stoneham, and M. Jaros, Phil. Mag. B **55**, 225 (1987).

[101] K. K. Ng, W. J. Polito, and J. R. Ligenza, Appl. Phys. Lett. **44**, 626 (1984).

[102] L. Ley, S. Kowalczyk, R. Pollak, D. A. Shirley, Phys. Rev. Lett. **29**, 1088 (1972)

[103] B. H. Bransden and C. H. Joachain, *Physics of atoms and molecules* (Longman Inc. 1983).

[104] S. T. Pantelides, *Deep centers in semiconductors* (Gordon and Breach 1986).

[105] T. Koopmans, Physica **1**, 104 (1933)

[106] P. W. Anderson, Phys. Rev. Lett. **34**, 953 (1975)

[107] L. Skuja, Solid State Comm. **84**, 613 (1992).

[108] L. Skuja, J. Non-Cryst. Solids **179**, 51 (1994).

[109] M. Stapelbroek et al., J. Non-Cryst. Solids **32**, 313 (1979)

[110] E. J. Friebele, D. L. Griscom and M. J. Marrone, J. Non-Cryst. Solids **71**, 133 (185)

[111] G. Pacchioni and G. Ierano, Phys. Rev. B **57**, 818 (1998)

[112] A. A. Wolf et al., J. Non-Cryst. Solids **56**, 349 (1983)

[113] C. M. Hartwig and L. A. Rahn, J. Chem. Phys., **67**, 4260 (1977)

[114] M. Cannas and M. Leone, J. Non-Cryst. Solids **280**, 183 (2001).

[115] D. S. Kliger, J. W. Davis and C. A. Randall, *Polarized Light in Optics and Spectroscopy* (Academic Press 1990).

[116] Y. Glinka, J. Exp. and Theor. Phys. **111**, 1748 (1997).